SANDIA REPORT

SAND96-2345 • UC-261
Unlimited Release
Printed September 1997

Predicting Aerodynamic Characteristics of Typical Wind Turbine Airfoils Using CFD

Walter P. Wolfe, Stuart S. Ochs

Prepared by
Sandia National Laboratories
Albuquerque, New Mexico 87185 and Livermore, California 94550

Sandia is a multiprogram laboratory operated by Sandia Corporation, a Lockheed Martin Company, for the United States Department of Energy under Contract DE-AC04-94AL85000.

Sandia National Laboratories

SF2900Q(8-81)

Issued by Sandia National Laboratories, operated for the United States Department of Energy by Sandia Corporation.

Available to DOE and DOE contractors from
Office of Scientific and Technical Information
P.O. Box 62
Oak Ridge, TN 37831

Prices available from (615) 576-8401, FTS 626-8401

Available to the public from
National Technical Information Service
U.S. Department of Commerce
5285 Port Royal Rd
Springfield, VA 22161

NTIS price codes
Printed copy: A03
Microfiche copy: A01

SAND96-2345
Unlimited Release
Printed September 1997

Distribution
Category UC-261

Predicting Aerodynamic Characteristics of Typical Wind Turbine Airfoils Using CFD

Walter P. Wolfe
Unsteady and Reactive Fluid Mechanics Department
Sandia National Laboratories
P. O. Box 5800
Albuquerque, New Mexico 87185-0836

and

Stuart S. Ochs
Aerospace Engineering Department
Iowa State University
Ames, IA 50011

Abstract

An investigation was conducted into the capabilities and accuracy of a representative computational fluid dynamics code to predict the flow field and aerodynamic characteristics of typical wind-turbine airfoils. Comparisons of the computed pressure and aerodynamic coefficients were made with wind tunnel data. This work highlights two areas in CFD that require further investigation and development in order to enable accurate numerical simulations of flow about current generation wind-turbine airfoils: transition prediction and turbulence modeling. The results show that the laminar-to-turbulent transition point must be modeled correctly to get accurate simulations for attached flow. Calculations also show that the standard turbulence model used in most commercial CFD codes, the k-ε model, is not appropriate at angles of attack with flow separation.

Acknowledgment

The authors wish to thank James Tangler of the National Renewable Energy Laboratory and Robyn Reuss Ramsay of Ohio State University for their assistance in obtaining the S809 wind tunnel data, Mark Rist of CFD Research Corporation for his assistance with CFD-ACE, and Todd Sterk, Sandia National Laboratories, for his assistance in digitizing the NACA 0021 aerodynamic data.

Table of Contents

List of Figures

List of Tables

Nomenclature

c	chord
C_d	drag coefficient = d/qS
C_l	lift coefficient = l/qS
C_m	moment coefficient about $0.25c$ = m/qcS
C_p	pressure coefficient = $(p\text{-}p_\infty)/q$
d	drag
l	lift
m	pitch moment
p	pressure
p_∞	freestream reference pressure
q	dynamic pressure = $\rho U_\infty^2/2$
U_∞	freestream velocity
u_τ	friction velocity = $\sqrt{\tau_w/\rho_w}$
x	axial coordinate from nose
y	normal coordinate from meanline
y^+	dimensionless sublayer distance from wall = $u_\tau y/\nu$
α	angle of attack
ν	kinematic viscosity
ρ	density
ρ_w	density at wall
τ_w	wall shear stress

Predicting Aerodynamic Characteristics of Typical Wind Turbine Airfoils Using CFD

Introduction

In the design of a commercially viable wind turbine, it is critical that the design team have an accurate assessment of the aerodynamic characteristics of the airfoils that are being considered. Errors in the aerodynamic coefficients will result in errors in the turbine's performance estimates and economic projections. The most desirable situation is to have accurate experimental data sets for the correct airfoils throughout the design space. However, such data sets are not always available and the designer must rely on calculations.

Methods for calculating airfoil aerodynamic characteristics range from coupled potential-flow/boundary-layer methods (e.g., VSAERO, 1994) to full-blown computational fluid dynamics (CFD) calculations of the Navier-Stokes equations. Potential-flow/boundary-layer methods are computationally efficient and yield accurate solutions for attached flow, but in general, they cannot be used for post-stall calculations. Some recent investigators have had limited success in developing empirical correlations to extend these types of codes into the post-stall region (e.g., Dini, *et al.*, 1995), however, this is still a research area and the technique has not yet been shown to be applicable to a wide range of airfoils.

Recent applications of CFD to solve the Navier-Stokes equations for wind-turbine airfoils are reflected in the works of Yang, *et al.* (1994, 1995) and Chang, *et al.* (1996). They used their in-house code to solve the 2-D flow field about the S805 and S809 airfoils in attached flow (Yang, *et al.*, 1994; Chang, *et al.*, 1996) and the S809 airfoil in separated flow (Yang, *et al.*, 1995). Computations were made with the Baldwin-Lomax (1978), Chein's (1982) low-Reynolds-number k-ε, and Wilcox's (1994) low-Reynolds-number k-ω turbulence models.

For angles of attack with attached flow, they generally obtained good agreement between calculated and experimental pressure coefficients. There was some underprediction of C_p over the forward half of the upper surface for both airfoils in vicinity of $\alpha = 5°$. In their 1994 work (Yang, *et al.*, 1994), they were able to get good agreement between the 5.13° experimental data and a calculation at $\alpha = 6°$ for the S805. This suggested experimental error as a possible explanation for the underprediction. However, since the same discrepancy occurs for the S809 airfoil (Chang, *et al.* 1996), the probability of experimental error is greatly reduced. (In this work, we offer a different explanation for this discrepancy.) As the flow begins to separate, they found that the Baldwin-Lomax turbulence model did a poor job of predicting the airfoil's pressure distribution. Both of the other models gave equally good C_p results, but the k-ω model had better convergence properties.

The majority of the published results of using CFD codes to calculate wind-turbine airfoil aerodynamic characteristics used in-house research codes that are not readily available to the typical wind turbine designer. In 1995, we began a limited investigation into the capabilities and accuracy of *commercially available* CFD codes for calculating the aerodynamic characteristics of wind-turbine airfoils. Because of the limited resources available, we limited our study to one CFD code and two airfoil sections, one laminar-flow and one primarily turbulent-flow airfoil. In the following, we present the results of this study. In this report, we do not show error bars on the experimental data since the original wind-tunnel data reports do not provide error estimates.

S809 Airfoil Section

For a typical horizontal-axis wind-turbine (HAWT) airfoil, we chose the S809. The S809 is a 21% thick, laminar-flow airfoil designed specifically for HAWT applications (Somers, 1997). A sketch of the airfoil is shown in Figure 1. A 600 mm-chord model of the S809 was tested in the 1.8 m × 1.25 m, low-turbulence wind tunnel at the Delft University of Technology. The results of these tests are reported by Somers (1997) and are used in this report for comparison with the numerical results. Another similarly sized model of the S809 was tested at Ohio State University (Gregorek, *et al.*, 1989). Our comparisons of the two experimental data sets showed that the results are essentially identical.

The experimental data show that at positive angles of attack below approximately 5°, the flow remains laminar over the forward half of the airfoil. It then undergoes laminar separation followed by a turbulent reattachment. As the angle of attack is increased further, the upper-surface transition point moves forward and the airfoil begins to experience small amounts of turbulent trailing-edge separation. At approximately 9°, the last 5% to 10% of the upper surface is separated. The upper-surface transition point has moved forward to approximately the leading edge. As the angle of attack is increased to 15°, the separated region moves forward to about the midchord. With further increases in angle of attack, the

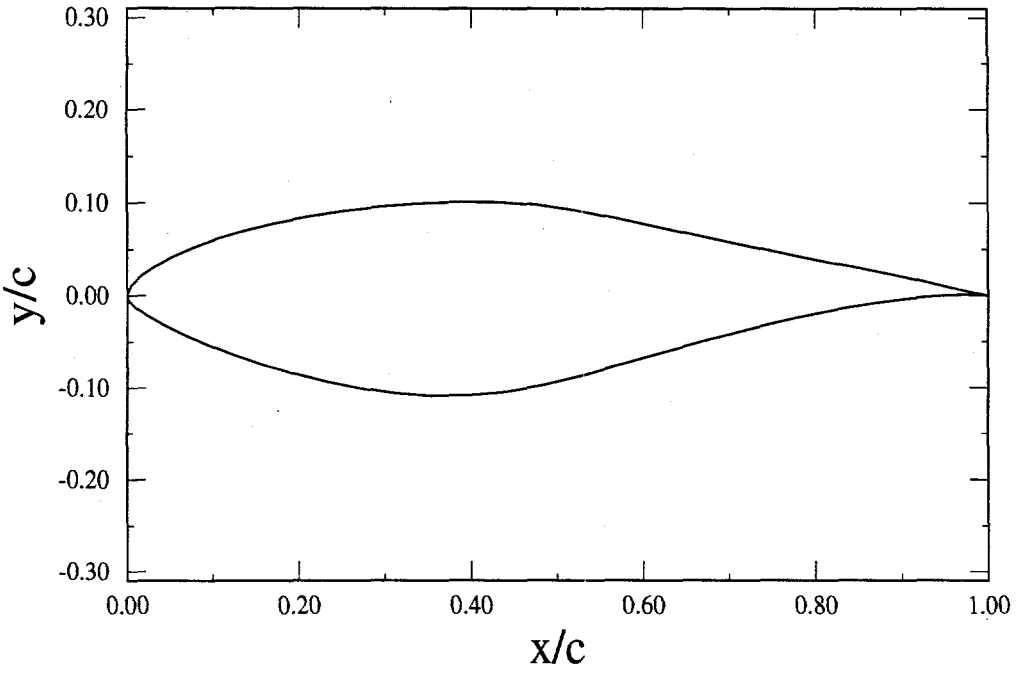

Figure 1. S809 Airfoil Profile

separation moves rapidly forward to the vicinity of the leading edge, so that at about 20°, most of the upper surface is stalled.

The S809 profile was developed using the Eppler design code (Eppler and Somers, 1980a, 1980b). Consequently, the surface profile is defined by a table of coordinates rather than by an analytical expression. To obtain the fine resolution needed for our numerical simulations, we interpolated between the defining surface coordinates using a cubic spline.

NACA 0021 Airfoil Section

The NACA 0021 airfoil is one of the NACA four-digit wing section series. It is a 21% thick, symmetrical airfoil with the point of maximum thickness located at $x/c = 0.30$, where x is the axial coordinate measured from the airfoil's nose and c is the chord length. A complete description of the airfoil can be found in Abbott and von Doenhoff (1959). Figure 2 shows the NACA 0021 profile.

The experimental data that are compared with the CFD calculations were taken from Gregorek, *et al.* (1989). An NACA 0021 airfoil section was tested in the OSU $6'' \times 22''$ trisonic wind tunnel at Mach = 0.20 and Reynolds number = 1.5×10^6. Surface pressures were measured with 56 taps distributed along the surface. Only the steady-state data are used for the following comparisons.

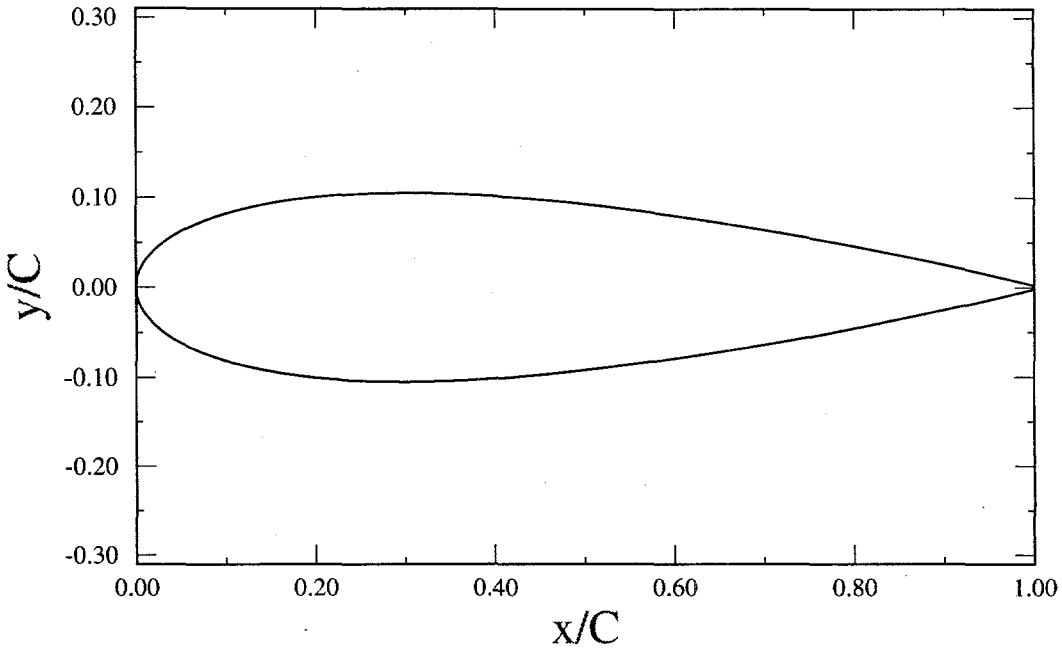

Figure 2. NACA 0021 Section Profile

CFD Code

Since we could examine only one code, we wanted a code with capabilities that were more or less representative of most commercial CFD codes. We looked for the capability to calculate incompressible, laminar/turbulent, 2-D/3-D, steady/unsteady flows, and to run on desk-top workstations. For our calculations, we used a SUN SPARC-10. Resource constraints forced us to look at codes that were currently licensed for Sandia's computing facilities. We made no effort to find the "best" CFD code for wind turbine applications.

Based on these criteria and constraints, we selected CFD-ACE for our studies. CFD-ACE is a computational fluid dynamics code that solves the Favre-averaged Navier-Stokes equations using the finite-volume approach on a structured, multi-domain, non-overlapping, non-orthogonal, body-fitted grid (CFDRC, 1993). The solution algorithms are pressure based. The code can solve laminar and turbulent, incompressible and compressible, 2-D and 3-D, steady and unsteady flows. Several turbulence models are available, including Baldwin-Lomax, Launder and Spalding k-ε, Chien low-Reynolds number k-ε, RNG* k-ε, and k-ω The default model is Launder and Spalding k-ε. During this investigation, we experienced problems with the

*Re-Normalization Group

k-ω model. CFDRC was able to duplicate our results and began an effort to identify and fix the problem. The k-ω model, therefore, was not available for this study. CFD-ACE has the capability to handle domain interfaces where the number of cells in adjacent domains are not equal, although each cell in the coarser-grid domain must exactly interface with an integer number of cells in the finer-grid domain. This capability was used in our simulations of mixed laminar/turbulent flow.

S809 Numerical Results

Our initial CFD simulations used a C-type grid topology with approximately 300 cells along the airfoil's surface and 24 cells normal to the surface. The normal grid spacing was stretched so that the cell thickness at the surface gave $y^+ \geq 30$. In the streamwise direction, the wake was modeled with 32 cells. The computational domain extended to 10 chord lengths from the body in all directions. Fully turbulent flow was assumed using the default k-ε turbulence model. All calculations were made at a Reynolds number of 2×10^6 and assumed incompressible flow.

Figures 3 through 5 show comparisons between the calculated and experimental surface pressure distributions for angles of attack of 0°, 1.02°, and 5.13°, respectively. The C_p comparisons for 0° and 1.02° show reasonably good agreement over the entire airfoil surface, except in the regions of the laminar separation bubbles. The experimental pressure distributions show the laminar separation bubbles just aft of the midchord on both the upper and lower surfaces. They are indicated by the experimental data becoming more-or-less constant with respect to x/c, followed by an abrupt increase in pressure as the flow undergoes turbulent reattachment. Since the calculations assume fully turbulent flow, no separation is indicated in the numerical results.

Figure 5 shows that the pressure comparison for 5.13° is good except over the forward half of the upper surface. Here the calculation is not adequately capturing the suction-side pressure. This is the same discrepancy found by Yang, *et al.* (1994) and Chang, *et al.* (1996).

Table 1 compares the aerodynamic coefficients for these same three cases. The predicted lift coefficients are accurate to within 10% and the moment coefficients to within 16%. The predicted drag coefficients are between 50% and 80% higher than the experiment results. This overprediction of drag was expected since the actual airfoil has laminar flow over the forward half.

Before proceeding with calculations at higher angles of attack, we made a more detailed analysis of the errors in the calculated pressure on the forward half of the upper surface for 5° angle of attack. In order to increase our confidence in the experimental data, we compared the data from Somers (1997) with data from Ohio State's tests (Gregorek, 1989). Figures 6 and 7 show comparisons for approximately 4° and 6° angle of attack. These figures show good agreement between the different experiments. This indicates that the data are correct and that the differ-

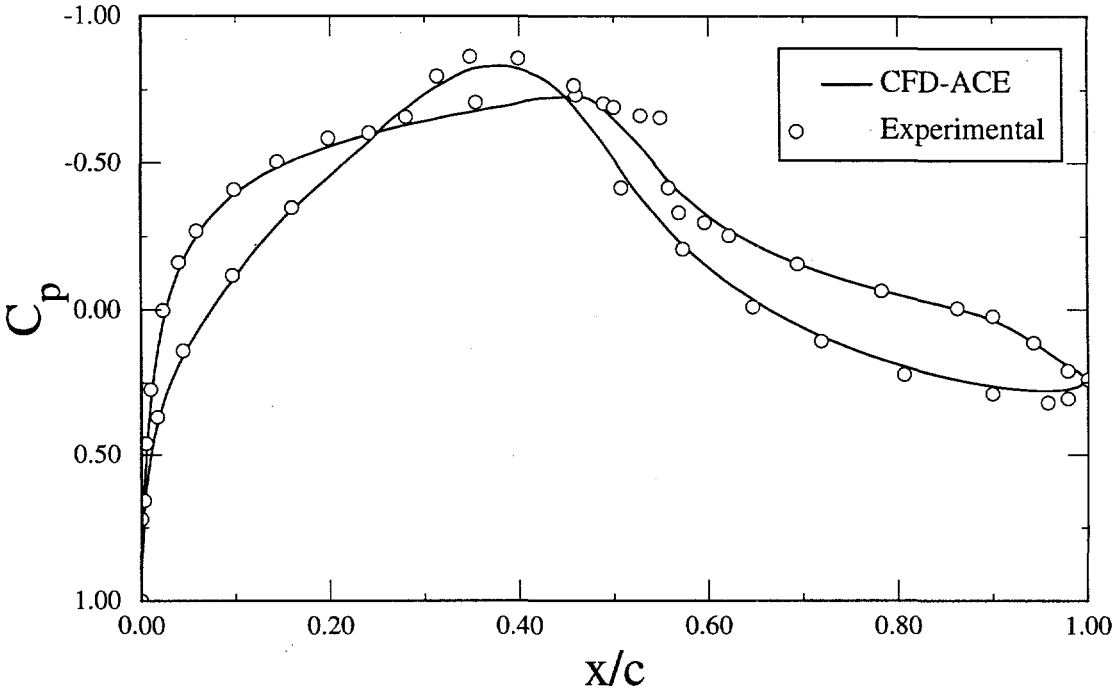

Figure 3. Pressure Distribution for S809 at $\alpha = 0°$, Fully Turbulent Calculation

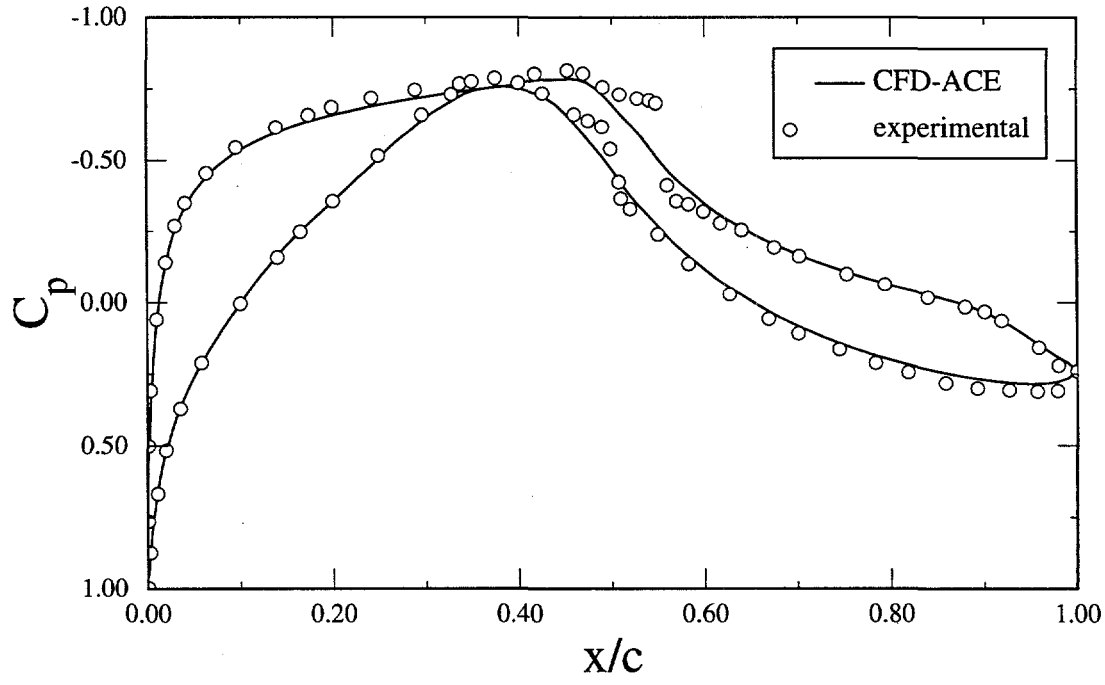

Figure 4. Pressure Distribution for S809 at $\alpha = 1.02°$, Fully Turbulent Calculation

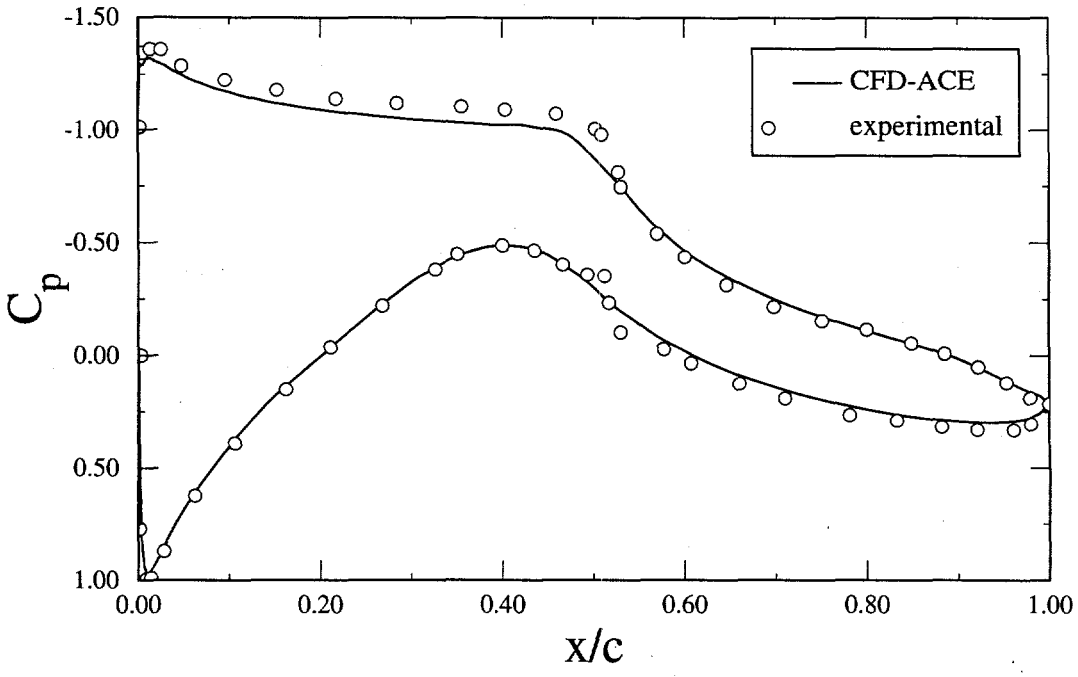

Figure 5. Pressure Distributions for S809 at $\alpha = 5.13°$, Fully Turbulent Calculation

Table 1: Comparisons Between S809 Calculated and Experimental Aerodynamic Coefficients, Fully Turbulent Calculations

α deg	C_l				C_d				C_m			
	calc	exp	error $\times 10^4$	% error	calc	exp	error $\times 10^4$	% error	calc	exp	error $\times 10^4$	% error
0	0.1324	0.1469	-145	-10	0.0108	0.0070	38	54	-0.0400	-0.0443	43	-10
1.02	0.2494	0.2716	-222	-8	0.0110	0.0072	38	53	-0.0426	-0.0491	65	-13
5.13	0.7123	0.7609	-486	-6	0.0124	0.0070	54	77	-0.0513	-0.0609	96	-16

ences between the calculated and experimental results are due to errors in the calculations.

We ran calculations with all of the available turbulence models and tried several grid refinements, especially around the nose. The results were essentially the same as those shown in Figure 5. To check the effects of the fully turbulent flow assumption, we also ran an Euler calculation at this angle of attack. The results are shown in Figure 8. This comparison shows very good agreement over the forward half of both the upper and lower surfaces, indicating that the disagreement in Figure 5 is a result of assuming turbulent flow over the forward half of the airfoil.

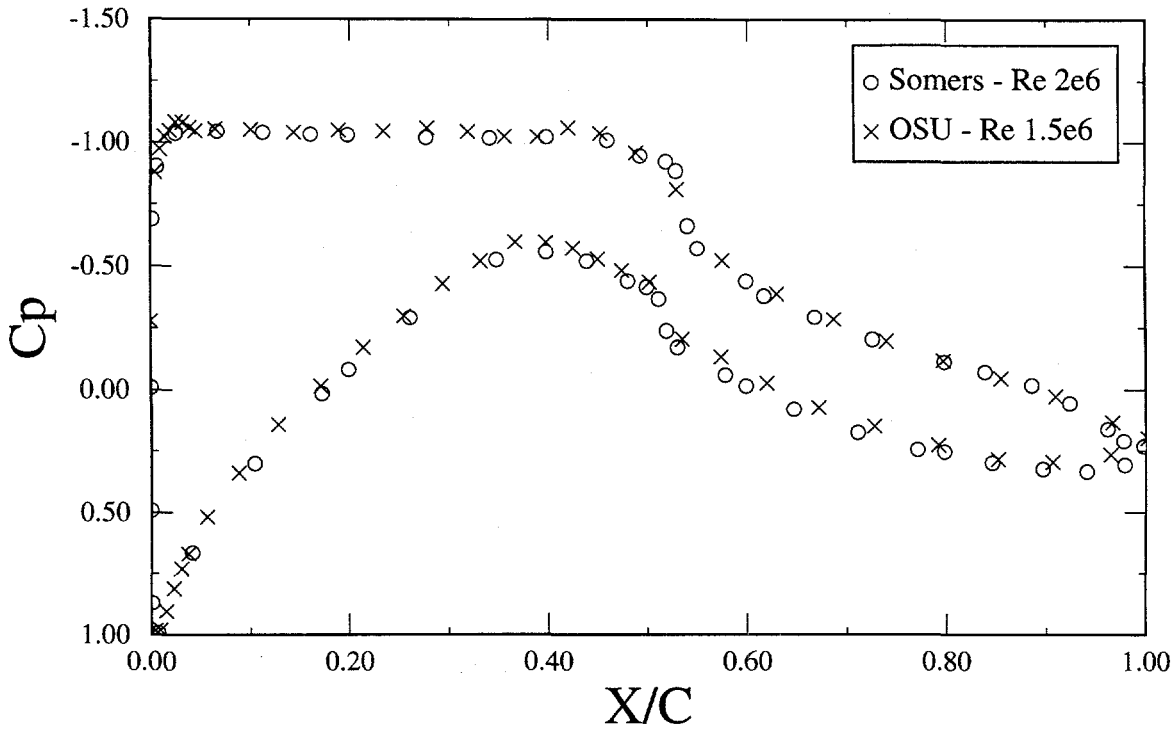

Figure 6. Comparison of Experimental Data for S809 at 4.1° Angle of Attack

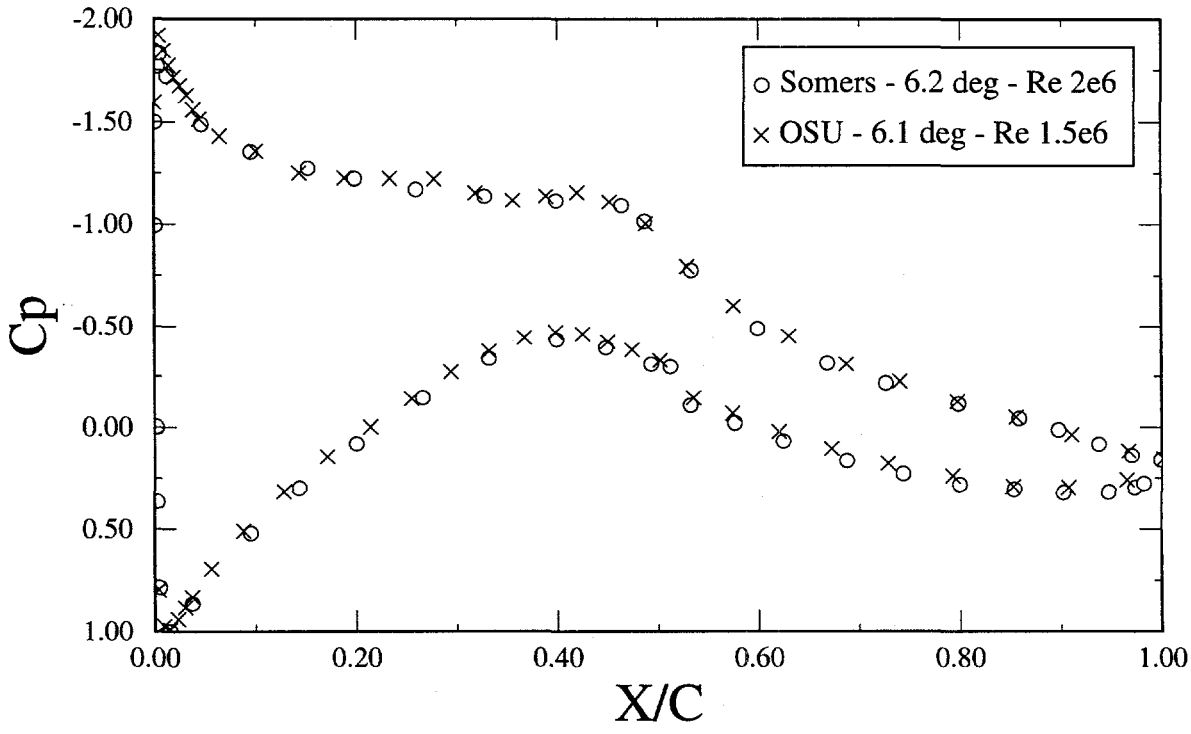

Figure 7. Comparison of Experimental Data for S809 at Approx. 6.2° Angle of Attack

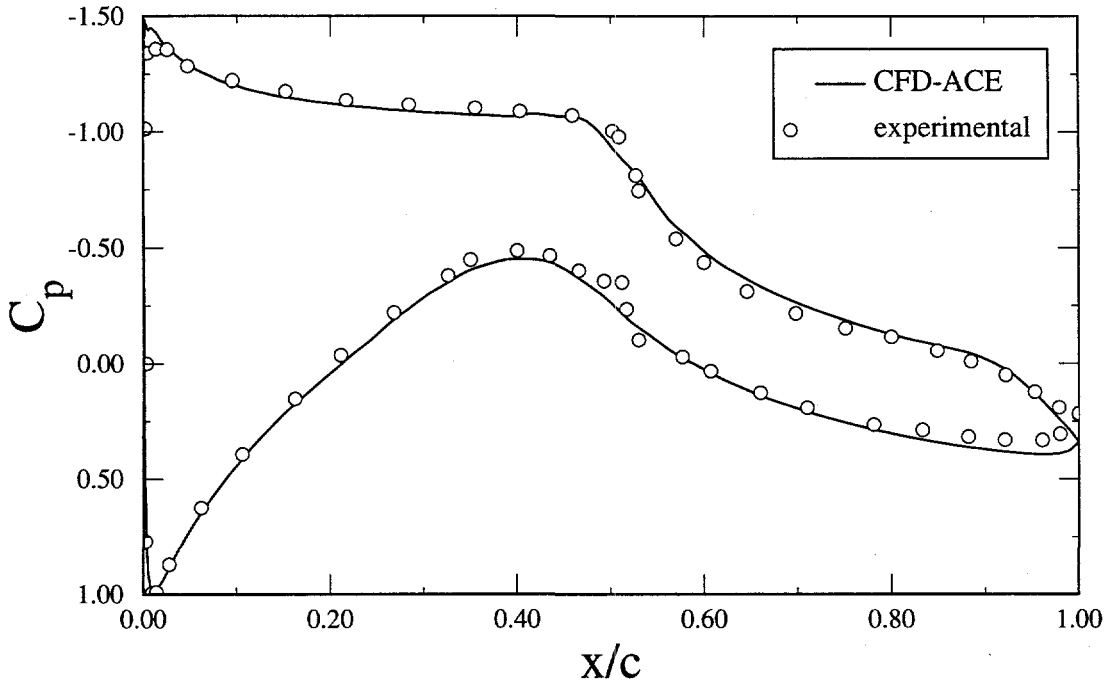

Figure 8. Pressure Distribution for S809 at $\alpha = 5.13°$, Euler Calculation

The pressure at the tail of the airfoil shows some error because the effect of the thickening boundary layer is not captured. We tried running a fully laminar calculation, but could not get a converged solution. The laminar flow separated on both surfaces at approximately the 50% chord positions, but because there was no turbulence model, it was unable to transition and reattach as occurs in the actual flow.

Both the S809 and the S805 airfoils have relatively sharp leading edges. At $\alpha = 5.13°$, the lower-surface stagnation point is displaced somewhat from the leading edge but is still relatively close. We believe that the problem with the calculations is that the turbulence models used for the calculations (both ours and those of Yang and Chang) cannot adequately capture the very rapid acceleration that occurs as the air flows from the stagnation point, around the airfoils' nose, to the upper surface.

After some thought and consultation with the staff at CFDRC, we decided that what was needed was the ability to simulate a mixture of both laminar and turbulent flow, i.e., we needed a good transition model in the code. This would allow us to more accurately predict the surface pressure and greatly improve the drag predictions. Unfortunately, we know of no good production transition models with universal applicability. To the best of our knowledge, no commercially available CFD code contains a transition model. CFDRC agreed to add the capability to run mixed laminar and turbulent flow by splitting the computational region into different domains and specifying laminar flow within certain domains. The remaining domains use the standard k-ε turbulence model. The disadvantages of this

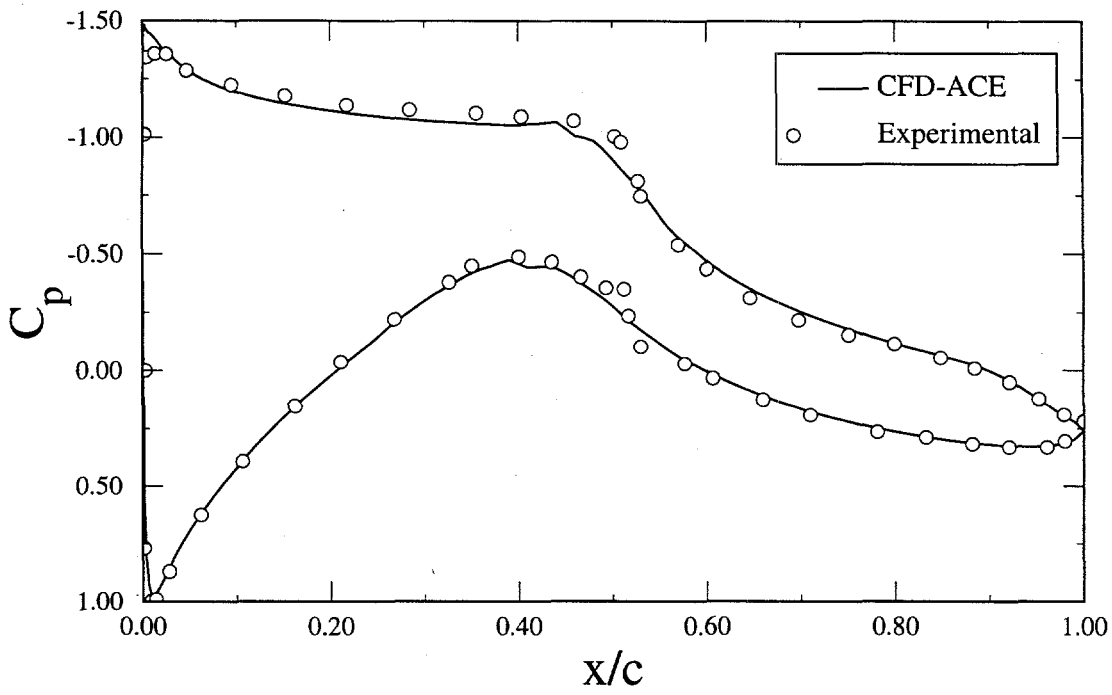

Figure 9. Pressure Distribution for S809 at $\alpha = 5.13°$, Mixed Laminar/Turbulent Calculation

approach are that the accuracy of the simulation depends on one's ability to accurately guess the transition location, and a new grid must be generated if one wants to change the transition location.

Figure 9 shows the comparison for surface pressure at $\alpha = 5.13°$ with this mixed laminar/turbulent model. This simulation used 324 cells along the airfoil surface and 32 cells normal to the surface in the laminar domain. The spacing normal to the wall was stretched to give $y^+ \leq 5$ in the laminar region and $y^+ \geq 30$ in the turbulent regions. This change in the cell thickness at the wall is necessary because laminar flow is calculated up to the wall, while turbulent flow using the k-ε turbulence model uses wall functions within the cell at the wall. The transition locations on both the upper and lower surfaces were specified at the locations of maximum thickness as measured from the mean line; $x/c = 0.45$ on the upper surface and $x/c = 0.40$ on the lower surface. The "wiggles" in the calculated pressure curves at these points are an artifact of the domain interface where four cells in the laminar domain interface with one cell in the turbulent domain.

The pressure coefficients are in very good agreement over the full airfoil surface, except for a small region on the upper-surface leading edge where the pressure is underpredicted. We believe that this is due to a small inaccuracy in the leading edge radius. The table of defining surface coordinates (Somers, 1997) does not give sufficient definition of the S809 leading edge to accurately duplicate the leading edge radius of the experimental model. Table 2 shows the comparison of the aerodynamic coefficients. At 5°, the lift coefficient is now equal to the experi-

Table 2: Comparisons Between S809 Calculated and Experimental Aerodynamic Coefficients, Mixed Laminar/Turbulent Calculations

α deg	C_l				C_d				C_m			
	calc	exp	error $\times 10^4$	% error	calc	exp	error $\times 10^4$	% error	calc	exp	error $\times 10^4$	% error
0	0.1558	0.1469	89	6	0.0062	0.0070	-8	-11	-0.0446	-0.0443	-3	1
1.02	0.2755	0.2716	39	1	0.0062	0.0072	-10	-14	-0.0475	-0.0491	16	-3
5.13	0.7542	0.7609	-67	-1	0.0069	0.0070	-1	-1	-0.0586	-0.0609	23	-4
9.22	1.0575	1.0385	190	2	0.0416	0.0214	202	95	-0.0574	-0.0495	-79	16
14.24	1.3932	1.1104	2828	25	0.0675	0.0900	-225	-25	-0.0496	-0.0513	17	-3
20.15	1.2507	0.9113	3394	37	0.1784	0.1851	-67	-4	-0.0607	-0.0903	396	-33

mental value. The pitch moment has a 4% error, and the error in the calculated drag has been reduced to 1%. The errors in the coefficients at 0° and 1° have also been significantly reduced. These angles of attack were rerun using the same grid as for the 5° case.

These results emphasize the need for the inclusion of a good transition model in CFD calculations, especially for airfoils typical of those used for horizontal axis wind turbines. Without a transition model, accurate predictions of aerodynamic coefficients over the full range of angles of attack are not possible.

Figures 10 through 12 show the pressure distributions for angles of attack of 9.22°, 14.24°, and 20.15°, respectively. For these angles of attack, the upper-surface transition point was moved forward to the leading edge. The lower-surface transition point remained at $x/c = 0.40$. At 20.15°, the simulations were run fully turbulent. For 9.22°, the computed pressure distribution agrees well with the experiment except for approximately the last 10% of the trailing edge. The experimental data show that there is a small separation zone on the upper surface in this region. This separation was not predicted by the simulation. At 14.24° and 20.15°, there is considerable difference between the experimental and numerical results. The experimental data show that at 14.24° the aft 50% of the upper surface has separated flow. The calculations predict separation over only the aft 5%. At 20.15°, the flow is separated over most of the upper surface. The calculations predict separation on only the aft 50%.

The calculations of Yang, *et al.*, (1995) using the k-ω turbulence model were able to predict the separation at the trailing edge at $\alpha = 9.22°$. They did not run the $\alpha = 14.24°$ case. At $\alpha = 20.15°$, their calculated pressure distribution was essentially the same as that shown in Fig. 12.

These discrepancies between the experimental data and the calculations are also reflected in the aerodynamic coefficients in Table 2. Figures 13 through 15

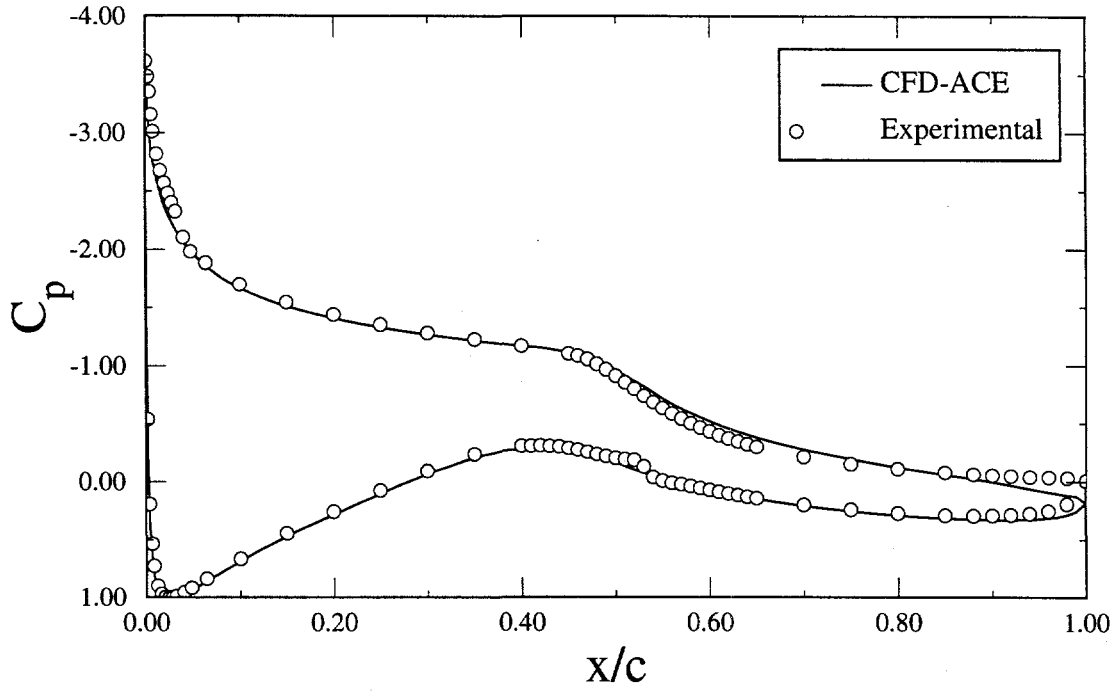

Figure 10. Pressure Distribution for S809 at $\alpha = 9.22°$, Mixed Laminar/Turbulent Calculation

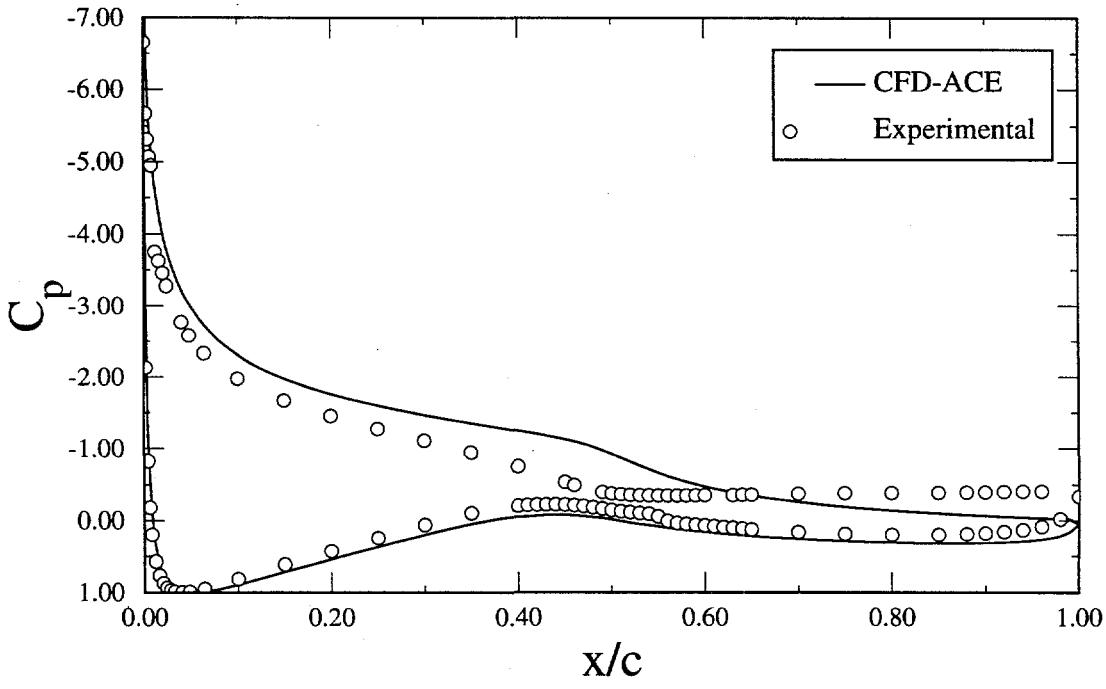

Figure 11. Pressure Distribution for S809 at $\alpha = 14.24°$, Mixed Laminar/Turbulent Calculation

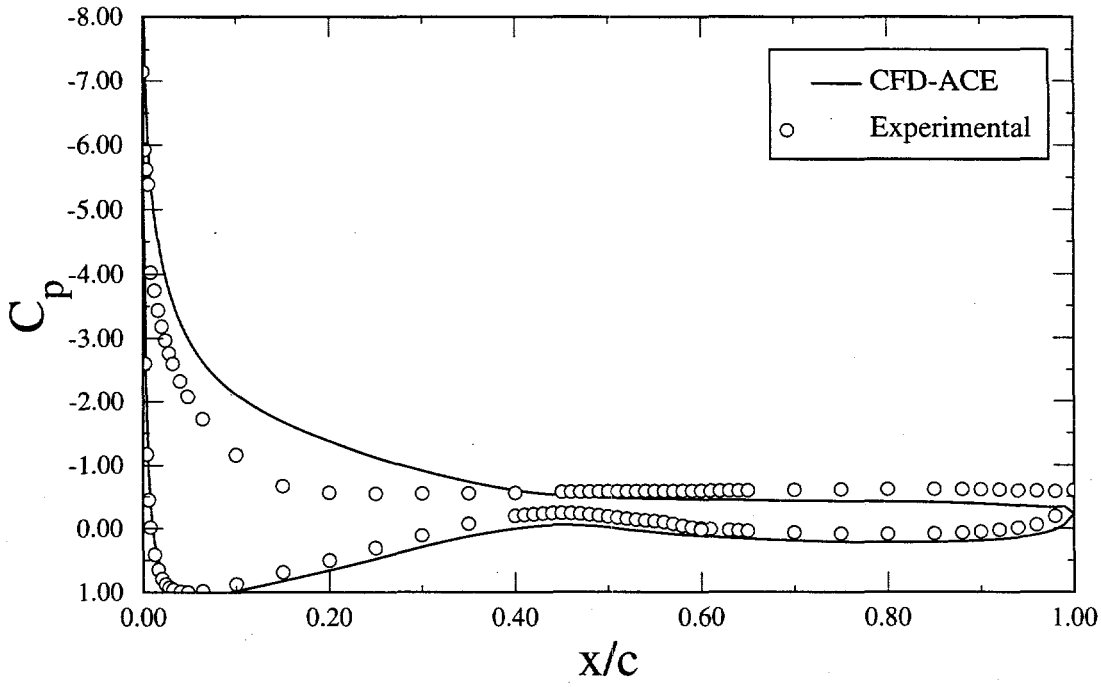

Figure 12. Pressure Distribution for S809 at $\alpha = 20.15°$, Fully Turbulent Calculation

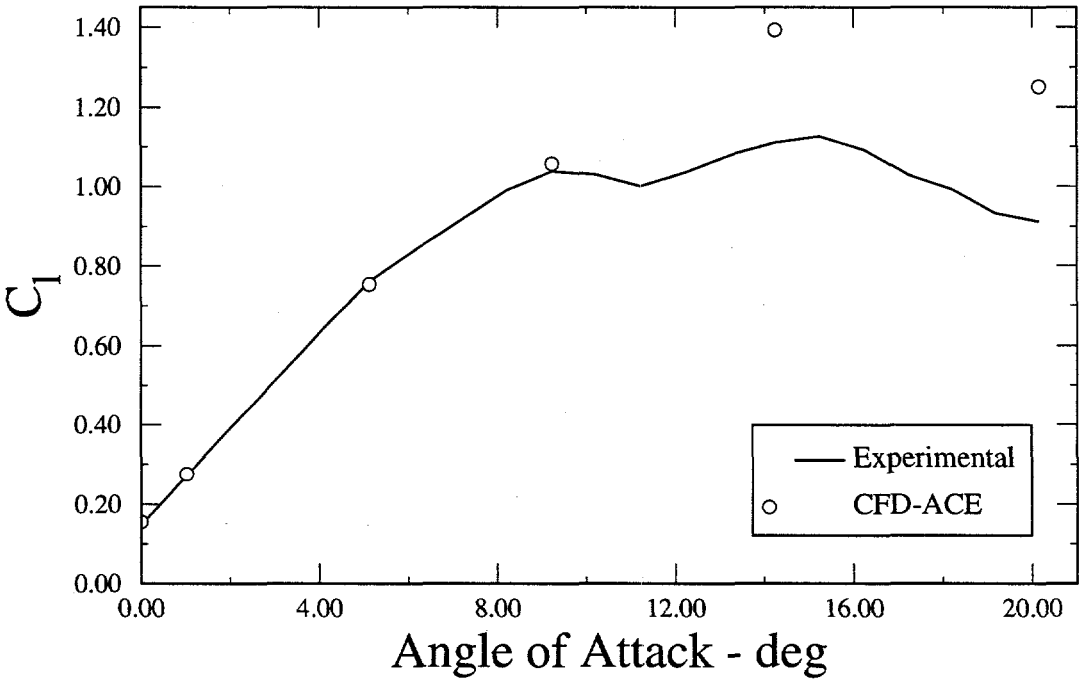

Figure 13. S809 Lift Coefficients

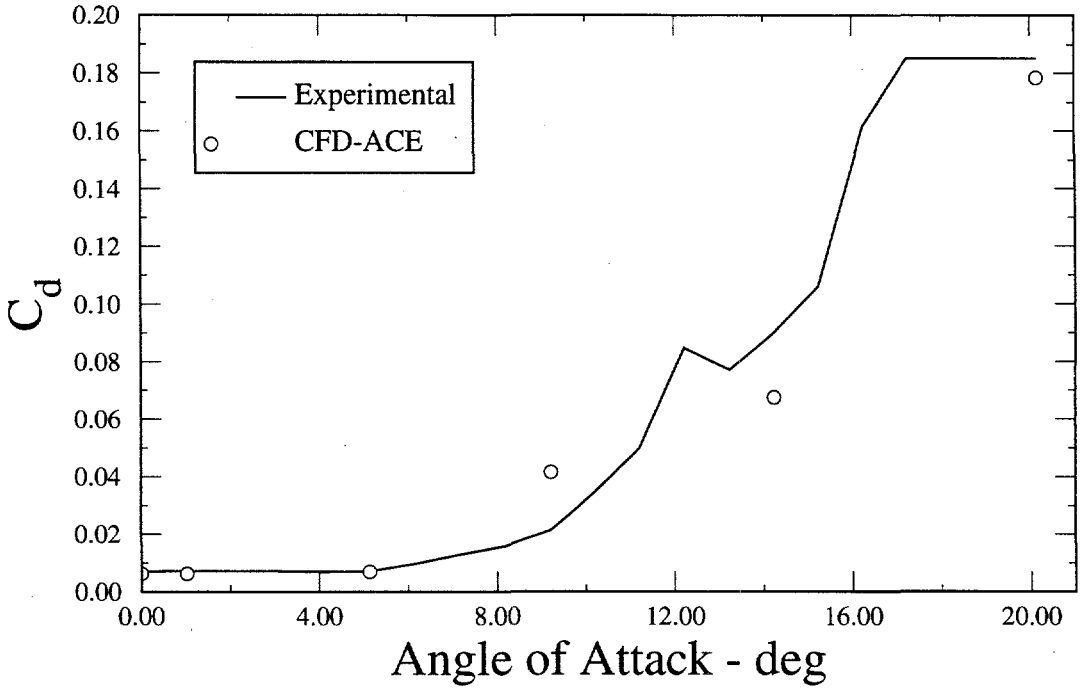

Figure 14. S809 Drag Coefficients

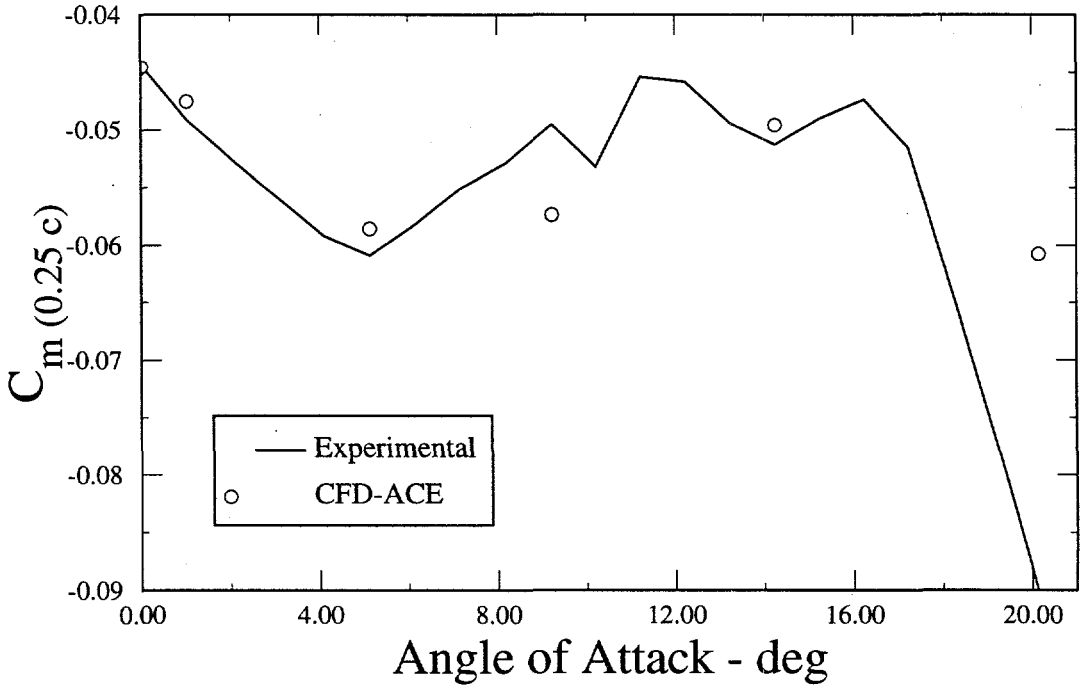

Figure 15. S809 Moment Coefficients About 0.25c

compare the numerical and experimental lift, drag, and moment coefficients, respectively. The calculated lift coefficients are accurate through approximately 9° angle of attack. Above this angle, the calculations do not pick up the airfoil's stall behavior and, therefore, overpredict the lift. The drag and pitch moment show similar behavior. The accuracy of the calculated pitching moment at $\alpha = 14.24°$ and the drag at $\alpha = 20.15°$ are more accidental than due to accurate modeling of the flow.

NACA 0021 Numerical Results

The computations for the NACA 0021 airfoil were made using a C-type grid that extended 10 chord lengths from the body in all directions. The direction normal to the body used 64 cells. The airfoil surface was modeled with a total of 256 cells, 128 cells each on the upper and lower surfaces. The wake was modeled with 64 cells. This gives a total of 20,480 cells in the computational domain. The y^+ values at the wall were adjusted to be consistent with the turbulence model that was used. For the k-ε model, $30 < y^+ < 60$. In laminar regions, $y^+ < 10$. All calculations assumed incompressible flow at a Reynolds number of 1.5×10^6.

Figure 16 shows the comparison between experimental data and the computations using the k-ε turbulence model. There were two experimental runs at these conditions, hence the two experimental data sets. This figure shows that the computed C_p's are somewhat lower than the experimental data. In order to determine the reason for this discrepancy, we also ran an Euler solution. The results of this run are shown in Fig. 17. The comparison looks similar to that in Fig. 16. We also tried a calculation using a mix of laminar and turbulent flow. The transition points were specified to be at the points of maximum thickness, $x/c = 0.30$. These results are shown in Fig. 18. Again, the comparison looks similar. Figure 19 shows a comparison of the results from all three calculations. They are essentially identical. These results show that the discrepancy between the calculated and experimental pressure coefficients is not due to presence of laminar flow over the forward portions of the airfoil. It is interesting to note that, unlike the S809, a transition model is not required for accurate C_p predictions.

A closer examination of the experimental data allows us to make some interesting observations. At $\alpha = 0°$, there are two data sets representing results from two separate runs (designated "a" and "b" in Figs. 16-18). The data show that there are some differences between the data from the different runs. However, the greatest differences are between data taken during the same run at the same chordwise station. An examination of the data plots in Gregorek, *et al.* (1989) shows that these differences occur between data taken on the upper and on the lower surfaces. Table 3 shows a comparison between pressure coefficients measured at two chordwise stations, $x/c = 0.08$ and $x/c = 0.20$. The differences between data taken on the same surfaces during different runs are all less than 6%. The lower surface has less difference than the upper surface. Within the same runs, however, the differences between data from the upper and lower surfaces range from 11% to 26%. One

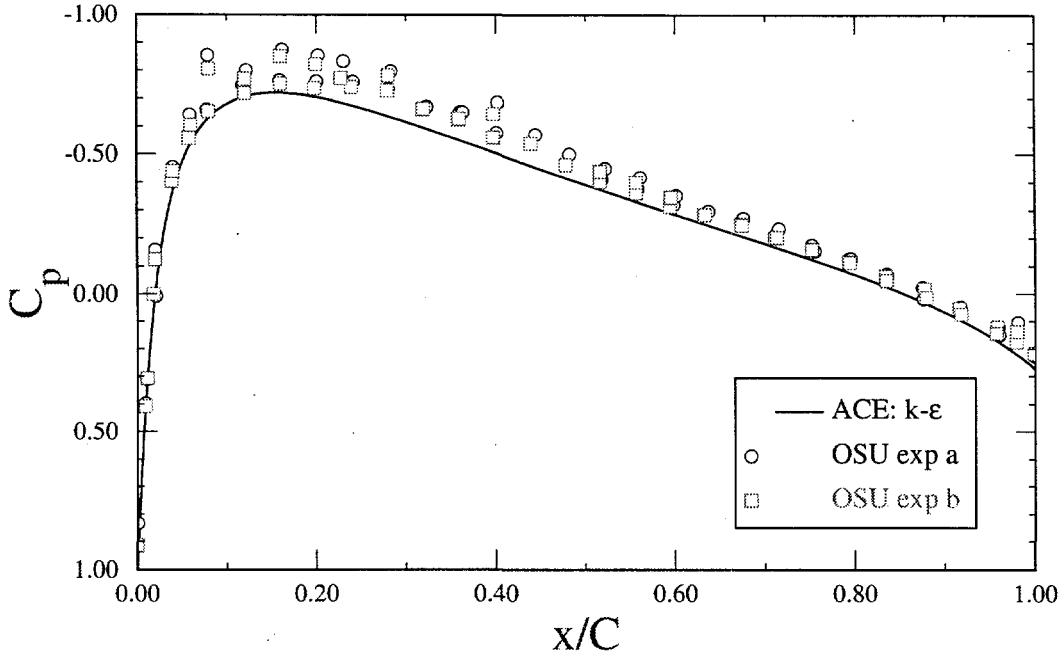

Figure 16. Pressure Coefficient Comparison for NACA 0021 at $\alpha = 0°$, k-ε Turbulence Model

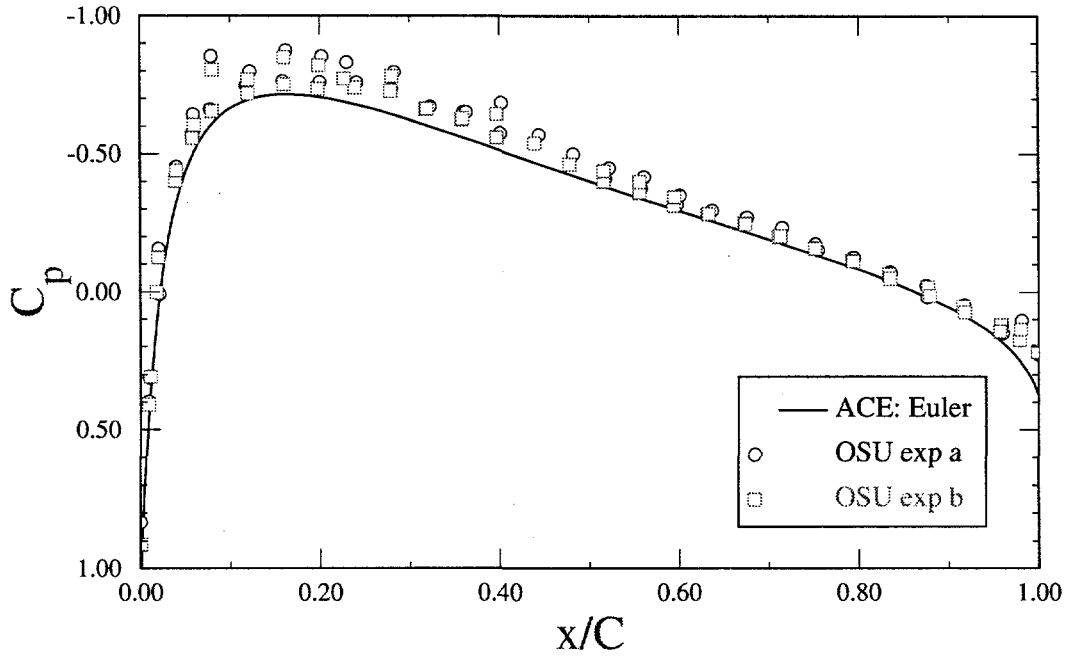

Figure 17. Pressure Coefficient Comparison for NACA 0021 at $\alpha = 0°$, Euler Calculation

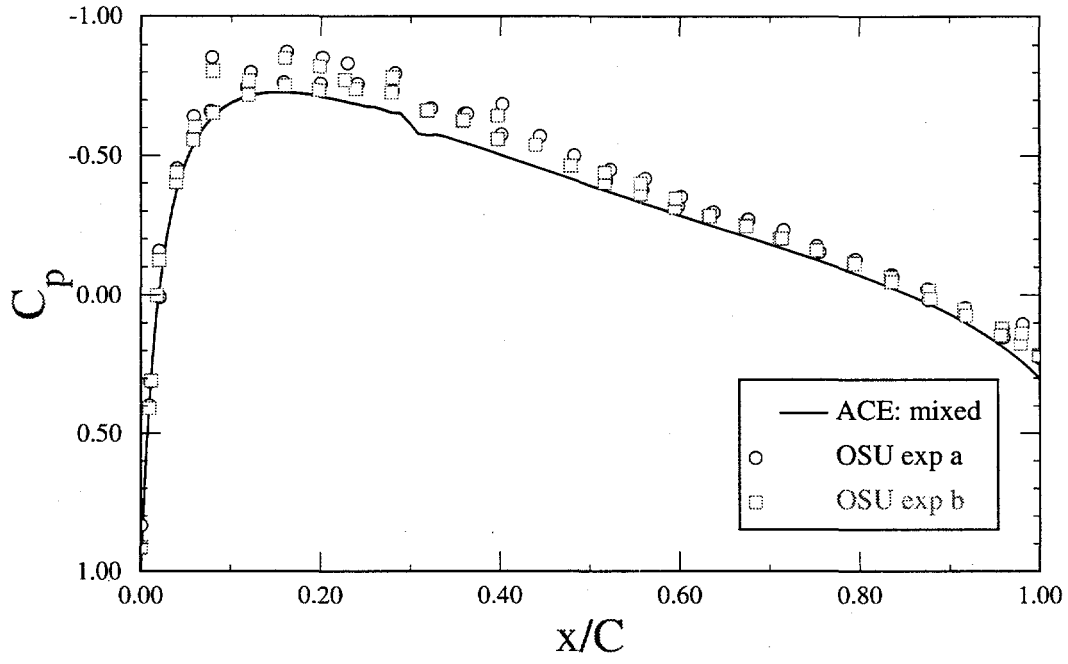

Figure 18. Pressure Coefficient Comparison for NACA 0021 at $\alpha = 0°$, Mixed Laminar and Turbulent Flow

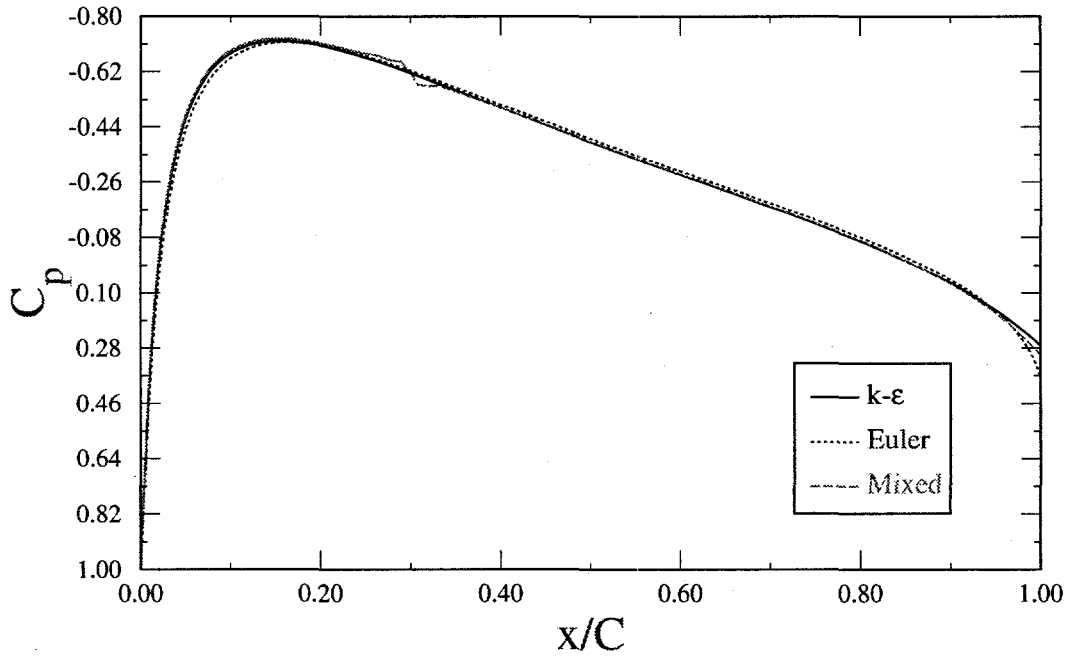

Figure 19. Pressure Coefficient Comparison for NACA 0021 at $\alpha = 0°$ for the Turbulent, Euler, and Mixed Laminar/Turbulent Calculations

Table 3: Pressure Coefficient Comparison Between Upper and Lower Surfaces and Between Runs for NACA 0021 at $\alpha = 0°$

	$x/c = 0.08$			$x/c = 0.20$		
	Upper Surface	Lower Surface	%-diff	Upper Surface	Lower Surface	%-diff
Run A	-0.854	-0.660	25.6	-0.853	-0.759	11.7
Run B	-0.805	-0.654	20.7	-0.821	-0.736	10.9
%-diff	5.9	0.9		3.8	3.1	

would not expect this magnitude of difference on a supposedly symmetrical model tested a 0° angle of attack. This leads us to suspect a problem with either the model, the pressure tap installation, or the instrumentation. At this time, there is no way to determine the cause.

Abbott and von Doenhoff (1959) provide some airfoil data derived from potential flow theory that can be used to estimate the pressure distribution about a NACA 0021 airfoil. Their theoretical results are compared with both the computed and experimental pressures in Fig. 20. Over the forward half of the airfoil, these theoretical data are in good agreement with the experimental data from the airfoil's lower surface. Over the aft half of the airfoil, these data deviate slightly from the experimental data. This is to be expected since the potential flow data do not account for the thickening boundary layer. From these comparisons, we conclude that the data from the lower surface appear to be accurate, while there is some error in the upper-surface data. The calculations do a reasonable job of computing the pressure distribution, although the code is again not computing the minimum suction peak correctly.

Figures 21 through 25 show comparisons between calculated and experimental pressure coefficients for angles of attack of 6°, 12°, 16°, 20°, and 45°, respectively. At $\alpha = 6°$ and 12°, the code does a reasonable accurate job of predicting C_p. At $\alpha = 16°$ and above, the quality of the agreement between calculation and experiment declines. From the experimental data at $\alpha = 12°$, there appears to be some flow separation over last 10-20% of the upper surface. At $\alpha = 16°$, the separation point has moved forward to approximately midchord. The separation point moves to about $x/c = 0.25$ at $\alpha = 20°$, and at $\alpha = 45°$, the flow separates at the leading edge. The code does not accurately predict separation for any of the angles of attack below 45°.

Figures 26 through 28 show comparisons for lift, drag, and moment coefficients, respectively. These same data are presented in tabular form in Table 4. These data show that below the point of flow separation, the predicted aerodynamic coefficients are not exact, but are reasonable. The %-errors are quite high at low angles of attack because the forces are very low. After the start of flow separation, however, the comparisons are very poor.

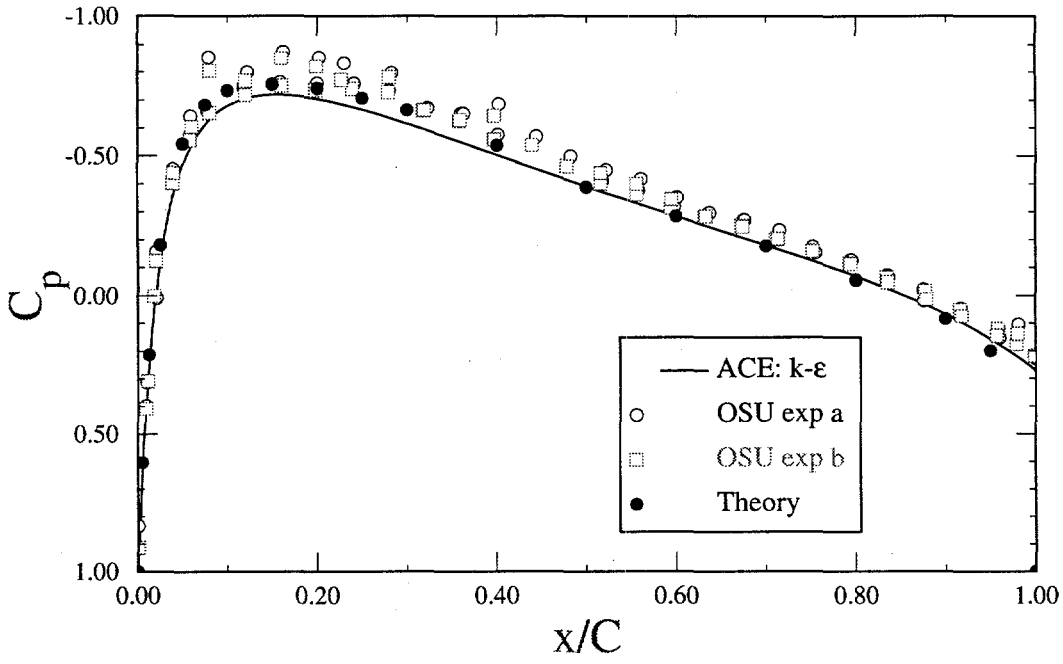

Figure 20. Comparison of Potential Flow Theory with Calculated and Experimental Results for NACA 0021 at $\alpha = 0°$

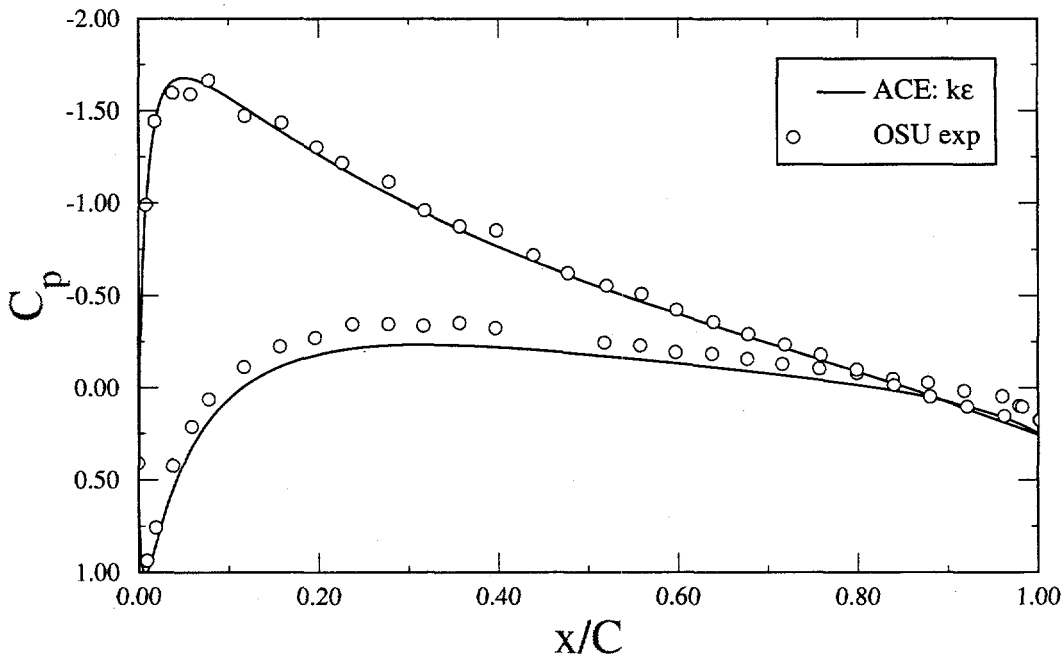

Figure 21. Pressure Coefficient Comparison for NACA 0021 at $\alpha = 6°$, *k*-ε Turbulence Model

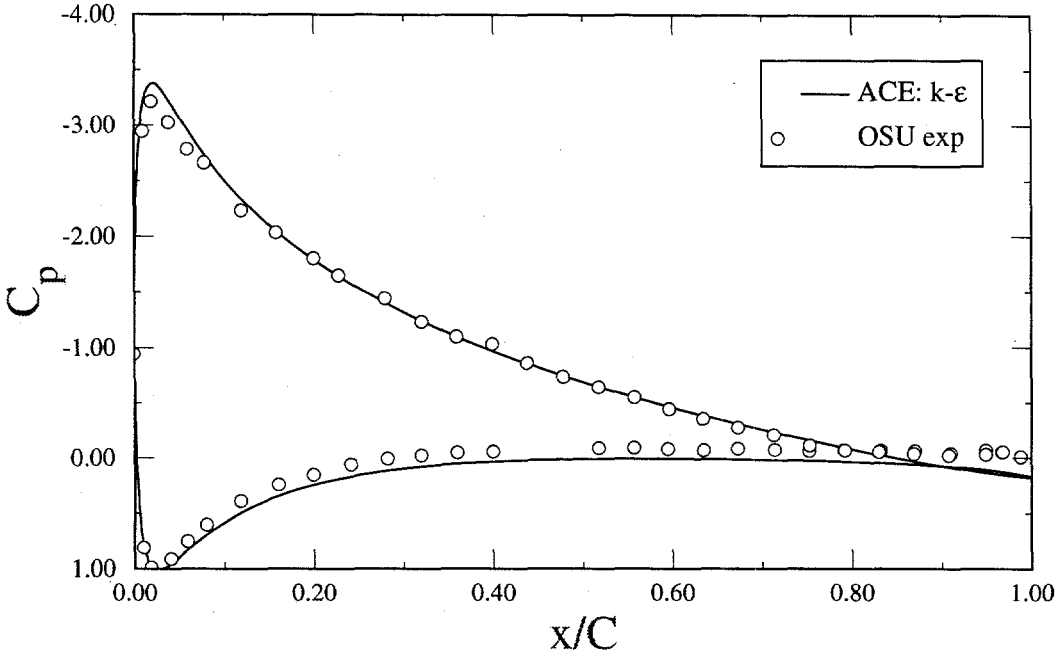

Figure 22. Pressure Coefficient Comparison for NACA 0021 at $\alpha = 12°$, k-ε Turbulence Model

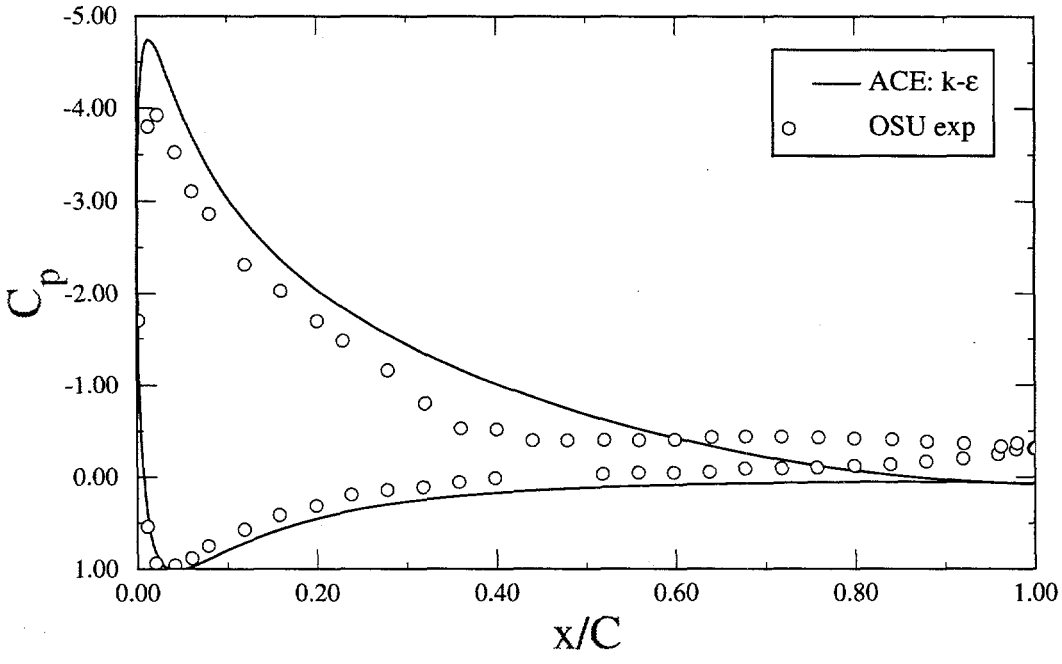

Figure 23. Pressure Coefficient Comparison for NACA 0021 at $\alpha = 16°$, k-ε Turbulence Model

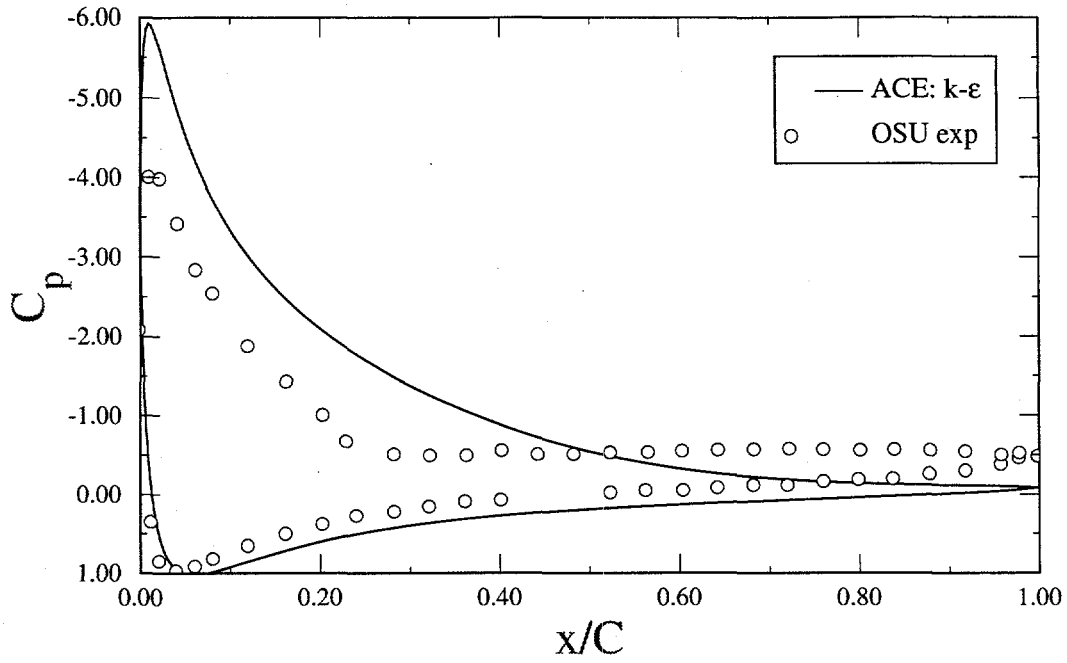

Figure 24. Pressure Coefficient Comparison for NACA 0021 at $\alpha = 20°$, k-ε Turbulence Model

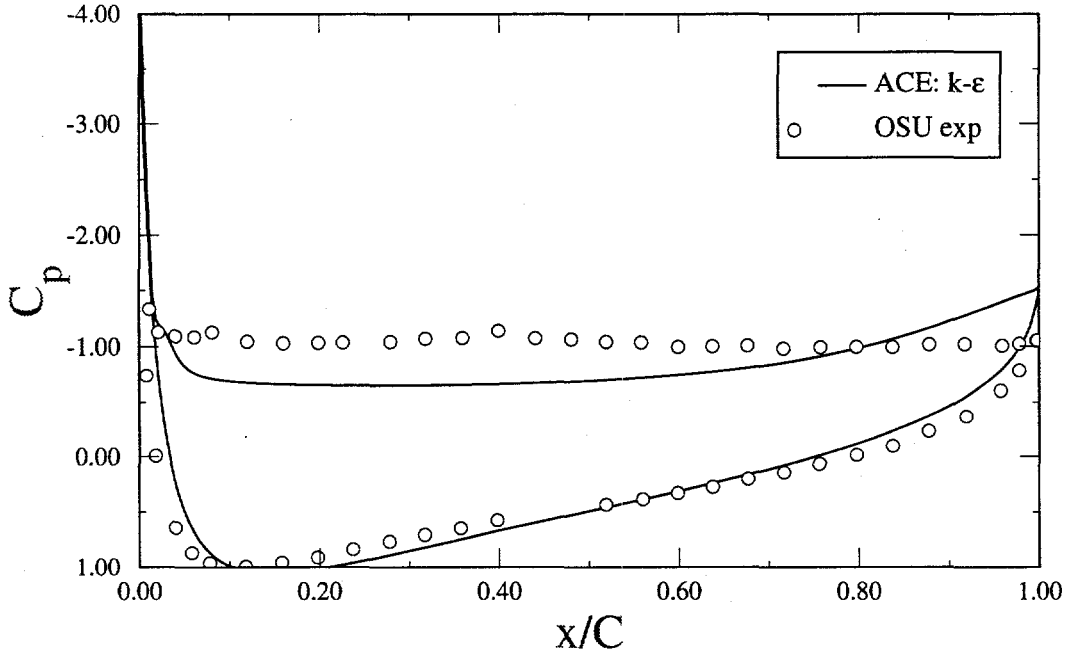

Figure 25. Pressure Coefficient Comparison for NACA 0021 at $\alpha = 45°$, k-ε Turbulence Model

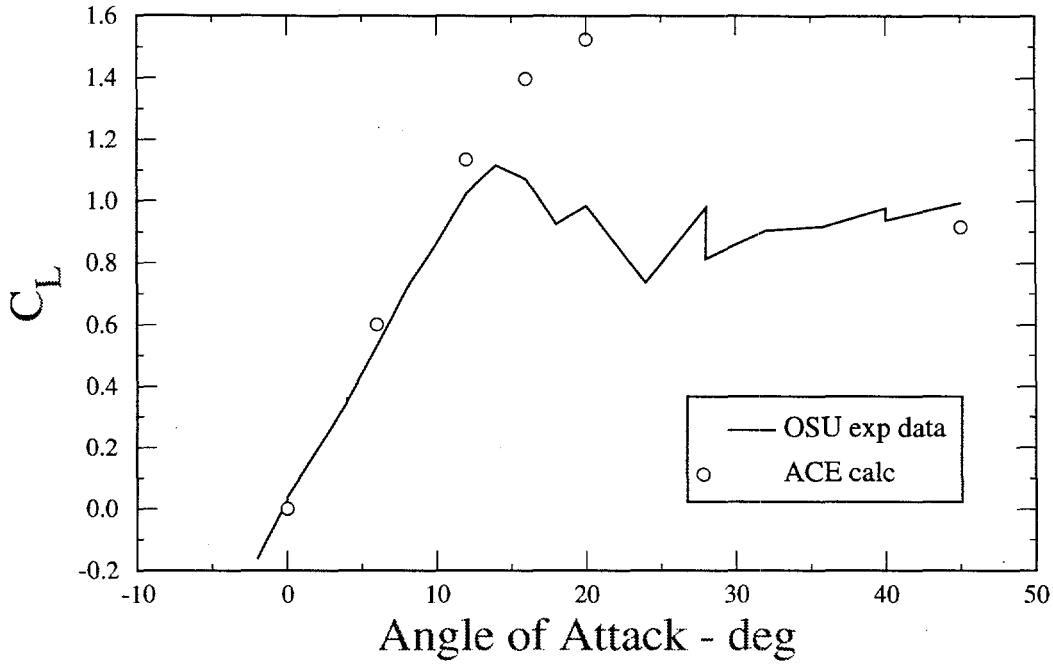

Figure 26. Comparison of NACA 0021 Calculated and Experimental Lift Coefficients

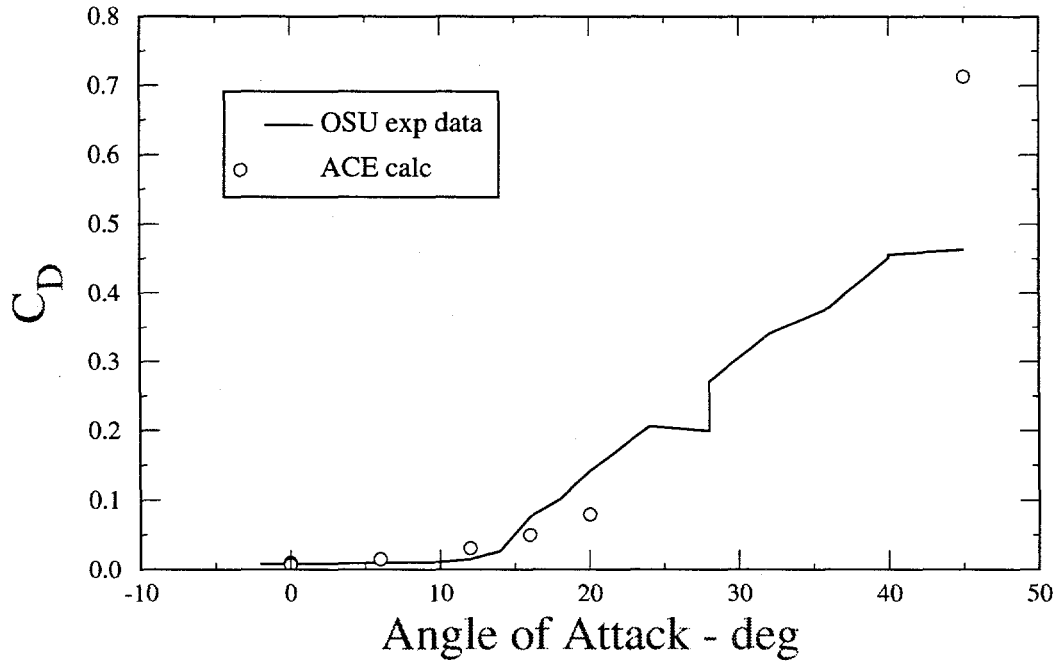

Figure 27. Comparison of NACA 0021 Calculated and Experimental Drag Coefficients

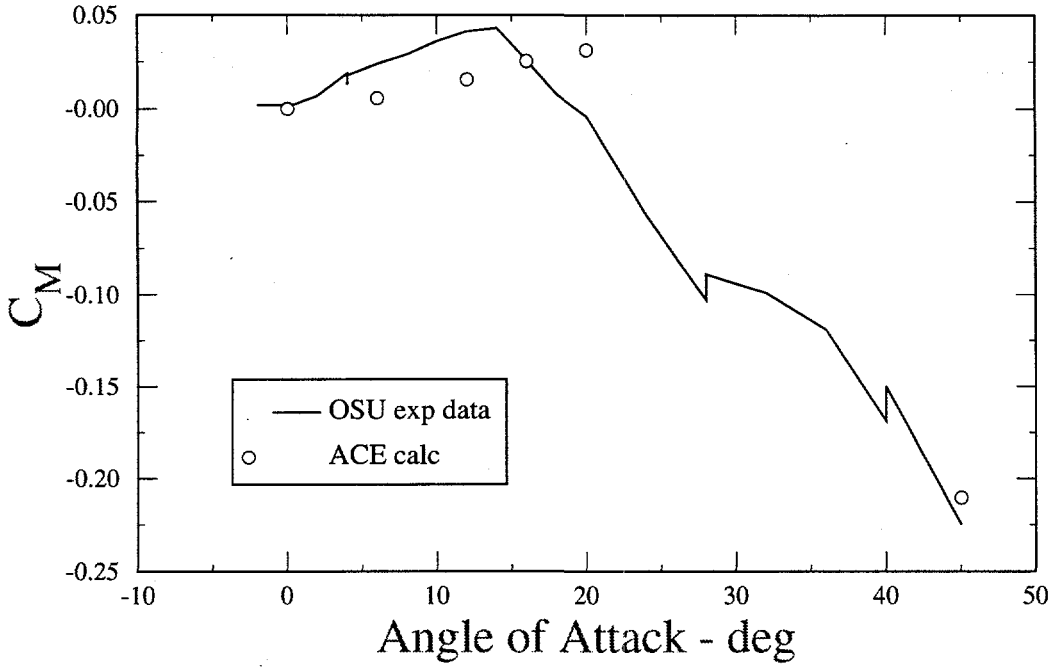

Figure 28. Comparison of NACA 0021 Calculated and Experimental Moment Coefficients

Table 4: Comparisons Between NACA 0021 Calculated and Experimental Aerodynamic Coefficients

α deg	C_l				C_d				C_m			
	calc	exp	error $\times 10^3$	% error	calc	exp	error $\times 10^4$	% error	calc	exp	error $\times 10^3$	% error
0	0.0005	0.033	-33	-98	0.0084	0.0082	2	2	-0.0001	0.0015	-2	-107
6	0.6012	0.528	73	14	0.0146	0.0095	51	54	0.0058	0.024	-21	-88
12	1.0575	1.025	110	11	0.0307	0.0148	159	107	0.0157	0.041	-25	-62
16	1.3980	1.071	327	31	0.0498	0.0768	-270	-35	0.0256	0.026	-0.0	-2
20	1.5237	0.984	540	55	0.0800	0.1413	-613	-43	0.0315	-0.004	36	886
45	0.9159	0.994	-78	-8	0.7132	0.4632	2500	54	-0.2103	-0.225	-15	-7

Summary and Conclusions

This report gives the results of our investigation into the capabilities and accuracy of a typical *commercially available* computational fluid dynamics code to predict the flow field and aerodynamic characteristics of wind-turbine airfoils. We have reaffirmed two areas in CFD that require further investigation and development in order to enable accurate numerical simulations of flow about current generation wind-turbine airfoils: transition prediction and turbulence modeling.

It must be noted that the calculations presented here were not blind calculations. We knew *a priori* the transition location from the experimental data and placed the computational transition as close as possible, consistent with numerical stability, to the actual locations. What these calculations show is that accurate predictions of the aerodynamic coefficients for attached flow are possible if one knows where the flow transitions. In an actual design environment, however, the designer would not know a priori the transition location, and would, therefore, need to make a reasonably accurate guess. This requires a designer with aerodynamic experience. What is really needed is an accurate, universally applicable transition model.

Horizontal axis wind turbines routinely operate in the post-stall regime, so accurate predications in this area are important. While this is a dynamic environment rather than a static one, we consider accurate static calculations a prerequisite to accurate dynamic calculations. We have shown that the default turbulence model in most CFD codes, the k-ε model, is not sufficient for accurate aerodynamic predictions at angles of attack in the post-stall region. This is understandable when one considers that the k-ε model uses wall functions based on the law of the wall and that the law of the wall does not hold for separated flows (Wilcox, 1994). An extensive investigation is required to determine the best transition and turbulence models for wind turbine applications.

References

I. H. Abbott and A. E. von Doenhoff 1959, *Theory of Wing Sections*, Dover Publications, New York, pp. 113-115, 326.

B. Baldwin and H. Lomax, 1978, "Thin Layer Approximation and Algebraic Model for Separated Turbulent Flows," AIAA-78-257.

CFDRC, 1993, *CFD-ACE Theory Manual*, ver. 1.0, CFD Research Corp., Huntsville, AL.

Y. L. Chang, S. L. Yang, and O. Arici, 1996, "Flow Field Computation of the NREL S809 Airfoil Using Various Turbulence Models," ASME, Energy Week-96, Book VIII, vol. I-Wind Energy, pp. 172-178.

K.-Y. Chien, 1982, "Predictions of Channel and Boundary-Layer Flows with a Low-Reynolds-Number Turbulence Model," *AIAA J.*, vol. 20, pp. 33-38.

P. Dini, D. P. Coiro, and S. Bertolucci, 1995, "Vortex Model for Airfoil Stall Predication Using an Interactive Boundary-Layer Method," ASME SED-Vol. 16, Wind Energy, pp. 143-147.

R. Eppler, and D. M. Somers, 1980a, "A Computer Program for the Design and Analysis of Low-Speed Airfoils," NASA TM-80210.

R. Eppler, and D. M. Somers, 1980b, "Supplement To: A Computer Program for the Design and Analysis of Low-Speed Airfoils," NASA TM-81862.

G. M. Gregorek, M. J. Hoffmann, and M. J. Berchak, 1989, "Steady State and Oscillatory Aerodynamic Characteristics of a NACA 0021 Airfoil: Data Report," Ohio State University, Columbus, OH.

D. M. Somers, 1997, "Design and Experimental Results for the S809 Airfoil," NREL/SR-440-6918, National Renewable Energy Laboratory, Golden, CO.

VSAERO, 1994, *VSAERO Users' Manual*, Rev. E.5, Analytical Methods Inc., Redmond, WA.

D. C. Wilcox, 1994, *Turbulence Modeling for CFD,* DCW Industries, Inc., La Cañada, CA.

S. L. Yang, Y. L. Chang, and O. Arici, 1994, "Incompressible Navier-Stokes Computation of the NREL Airfoils Using a Symmetric Total Variational Diminishing Scheme," *J. of Solar Energy Engineering*, vol. 116, pp. 174-182; also "Numerical Computation of the NREL Airfoils Using a Symmetric TVD Scheme," ASME, SED-Vol. 15, Wind Energy, 1994, pp. 41-49.

S. L. Yang, Y. L. Chang, and O. Arici, 1995, "Post-Stall Navier-Stokes Computations of the NREL Airfoil Using a k-ω Turbulence Model," ASME SED-vol. 16, Wind Energy, pp. 127-136.

Distribution

1 R. E. Akins
Washington & Lee University
P.O. Box 735
Lexington, VA 24450

1 H. Ashley
Dept. of Aeronautics and
Astronautics Mechanical Engr.
Stanford University
Stanford, CA 94305

1 E. Ausman
Polarconsort Alaska
1503 W. 33rd Avenue, Suite 310
Anchorage, AK 99530

1 B. Bell
Enron Wind Eneergy Systems
13000 Jameson Road
P.O. Box 1910
Tehachapi, CA 93561

1 K. Bergey
University of Oklahoma
Aero Engineering Department
Norman, OK 73069

1 C. P. Butterfield
NREL
1617 Cole Boulevard
Golden, CO 80401

1 G. Bywaters
New World Power Technology Center
Box 999
Waitsfield,VT 05673

1 J. Cadogan
U.S. Department of Energy
Office of Photovoltaic & Wind Tech.
Energy Efficiency & Renewable Energy, E-11
1000 Independence Avenue SW
Washington, DC 20585

1 J. Chapman
OEM Development Corp.
840 Summer St.
Boston, MA 02217-1533

1 R. N. Clark
USDA
Agricultural Research Service
P.O. Drawer 10
Bushland, TX 79012

1 J. Cohen
Princeton Economic Research, Inc.
1700 Rockville Pike, Suite 550
Rockville, MS 20852

1 C. Coleman
Northern Power Systems
Box 659
Moretown, VT 05660

1 R. Davis
Convergence Engineering Co.
5056 Sunrise Blvd, Suite B3
Fair Oaks, CA 95628

1 A. K. J. Deering
The Wind Turbine Company
515 116th Avenue NE, No. 263
Bellevue, WA 98004

1 E. A. DeMeo
Electric Power Research Institute
3412 Hillview Avenue
Palo Alto, CA 94304

1 A. J. Eggers, Jr.
RANN, Inc.
260 Sheridan Ave., Suite 414
Palo Alto, CA 94306

1 D. M. Eggleston
DME Engineering
P.O. Box 5907
Midland, TX 79704-5907

1 P. R. Goldman, Acting Deputy Director
Office of Photovoltaic & Wind Technology
Energy Efficiency & Renewable Energy,
EE-11
U.S. Department of Energy
1000 Independence Avenue
Washington, DC 20585

1 G. Gregorek
Aeronautical & Astronautical Dept.
Ohio State University
2300 West Case Road
Columbus, OH 43220

1 C. Hansen
University of Utah
Department of Mechanical Engineering
Salt Lake City, UT 84112

1 L. Helling
Librarian
National Atomic Museum
Albuquerque, NM 87185

1 S. Hock
Wind Energy Program
NREL
1617 Cole Boulevard
Golden, CO 80401

1 W. E. Holley
3731 Oak Brook Court
Pleasanton, CA 94588

1 B. J. Im
McGillim Research
11299-C San Pablo Avenue
El Cerrito CA 94530

1 K. Jackson
Dynamic Design
123 C Street
Davis, CA 95616

1 G. James
Dept. of Mechanical Engineering
University of Houston
4800 Calhoun
Houston, TX 77204-4792

1 O. Krauss
Division of Engineering Research
Michigan State University
East Lansing, MI 48825

1 R. Lynette
AWT/RLA
425 Pontius Avenue North, Suite 150
Seattle, WA 98109

1 D. Malcolm
Advanced Wind Turbines, Inc.
425 Pontius Avenue North, Suite 150
Seattle, WA 98109

1 J. F. Mandell
Montana State University
302 Cableigh Hall
Bozeman, MT 59717

1 T. McCoy
R. Lynette & Associates, Inc.
15042 N.E. 40th Street, Suite 206
Richmond, WA 09063

1 R. N. Meroney
Dept. of Civil Engineering
Colorado State University
Fort Collins, CO 80521

1 P. Migliore
NREL
1617 Cole Boulevard
Golden, CO 80401

1 A. Mikhail
Enron Energy Systems
13000 Jameson Road
P.O. Box 1910
Tehachapi, CA 93561

1 L. S. Miller
Aero Engineering Department
Wichita State University
Wichita, KS 67260-0044

1 W. Musial
NREL
1617 Cole Boulevard
Golden, CO 80401

1 NWTC Library
NREL
1617 Cole Boulevard
Golden, CO 80401

1 V. Nelson
Department of Physics
West Texas State University
P.O. Box 248
Canyon, TX 79016

1 G. Nix
NREL
1617 Cole Boulevard
Golden, CO 80401

5 S. S. Ochs
Iowa State University
Aerospace Engineering Department
Ames, IA 50011

1 J. Oler
Mechanical Engineering Dept.
Texas Tech University
P.O. Box 4289
Lubbock, X 79409

1 R. Osgood
NREL
1617 Cole Boulevard
Golden, CO 80401

1 M. Papadakis
Aero Engineering Department
Wichita State University
Wichita, KS 67260-0044

1 C. Paquette
The American Wind Energy Association
122 C Street NW, Fourth Floor
Washington, DC 20002

1 R. G. Rajagopalan
Aerospace Engineering Department
Iowa State University
404 Town Engineering Bldg.
Ames, IA 50011

1 M. C. Robinson
NREL
1617 Cole Boulevard
Golden, CO 80401

1 D. Sanchez
U.S. Dept. of Energy
Albuquerque Operations Office
P.O. Box 5400
Albuquerque, NM 87185

1 L. N. Sankar
Georgia Institute of Technology
School of Aerospace Engineering
Atlanta, GA 30332

1 L. Schienbein10/95
CWT Technologies, Inc.
4006 S. Morain Loop
Kennewick, WA 99337

1 T. Schweizer
Princeton Economic Research, Inc.
1700 Rockville Pike, Suite 550
Rockville, MD 20852

1 J. Sladky, Jr.
Kinetics Group, Inc.
P.O. Box 1071
Mercer Island, WA 98040

1 L. H. Soderholm
Agricultural Engineering, Room 213
Iowa State University
Ames, IA 50010

1 K. Starcher
AEI
West Texas State University
P.O. Box 248
Canyon, TX 79016

1 W. J. Steeley
Pacific Gas and Electric Co.
3400 Crow Canyon Road
San Ramon, CA 94583

1 F. S. Stoddard
Dynamic Design-Atlantic Office
P.O. Box 1373
Amherst, MA 01004

1 A. Swift
University of Texas at El Paseo
320 Kent Ave.
El Paso, TX 79922

1 J. L. Tangler
NREL
1617 Cole Boulevard
Golden, CO 80401

1 W. V. Thompson
410 Ericwood Court
Manteca, CA 95336

1 R. W. Thresher
NREL
1617 Cole Boulevard
Golden, CO 80401

1 K. J. Touryan
NREL
1617 Cole Boulevard
Golden, CO 80401

1 W. A. Vachon
W. A. Vachon & Associates
P.O. Box 149
Manchester, MA 01944

1 B. Vick
USDA, Agricultural Research Service
P.O. Drawer 10
Bushland, TX 79012

1 L. Wendell
2728 Enterprise Dr.
Richland, WA 99325

1 W. Wentz
Aero Engineering Department
Wichita State University
Wichita, KS 67208

1 R. E. Wilson
Mechanical Engineering Dept.
Oregon State University
Corvallis, OR 97331

1 S. R. Winterstein
Civil Engineering Department
Stanford University
Stanford, CA 94305

1 B. Wolff
Renewable Energy Program Manager
Conservation and Renewable Energy System
6918 NE Fourth Plain Boulevard, Suite B
Vancouver, WA 98661

1 M. Zuteck
MDZ Consulting
931 Grove Street
Kemah, TX 77565

1 S. Schuck Henry
Renewable Technology
Pacific Power
P.O. Box 5257
GPO Sydney, New South Wales 2001
AUSTRALIA

1 V. Lacey
Indal Technologies, Inc.
3570 Hawkestone Road
Mississauga, Ontario L5C 2V8
CANADA

1 A. Laneville
Faculty of Applied Science
University of Sherbrooke
Sherbrooke, Quebec J1K 2R1
CANADA

1 B. Masse
Institut de Recherche d'Hydro-Quebec
1800, Montee Ste-Julie
Varennes, Quebec J3X 1S1
CANADA

1 I. Paraschivoiu
Dept. of Mechanical Engineering
Ecole Polytechnique
CP 6079
Succursale A
Montreal, Quebec H3C 3A7
CANADA

1 R. Rangi
Manager, Wind Technology
Dept. of Energy, Mines and Resources
580 Booth 7th Floor
Ottawa, Ontario K1A 0E4
CANADA

1 P. Vittecoq
Faculty of Applied Science
University of Sherbrooke
Sherbrooke, Quebec J1K 2R1
CANADA

1 P. H. Madsen
Riso National Laboratory
Postbox 49
DK-4000 Roskilde
DENMARK

1 T. F. Pedersen
Riso National Laboratory
Postbox 49
DK-4000 Roskilde
DENMARK

1 M. Pedersen
Technical University of Denmark
Fluid Mechanics Dept.
Building 404
Lundtoftevej 100
DK 2800 Lyngby
DENMARK

1 A. F. Abdel Azim El-Sayed
Dept. of Mechanical Design &
Power Engineering
Zagazig University
3 El-lais Street
Zeitun
Cairo 11321
EGYPT

1 M. Anderson
Renewable Energy Systems, Ltd.
Eaton Court, Maylands Avenue
Hemel Hempstead
Herts HP2 7DR
ENGLAND

1 M. P. Ansell
School of Material Science
University of Bath
Claverton Down
Bath BA2 7AY
Avon
ENGLAND

1 A. D. Garrad
Garrad Hassan
9-11 Saint Stephen Street
Bristol BS1 1EE
ENGLAND

1 D. I. Page
Energy Technology Support Unit
B 156.7 Harwell Laboratory
Oxfordshire, OX11 ORA
ENGLAND

1 D. Sharpe
Dept. of Aeronautical Engineering
Queen Mary College
Mile End Road
London, E1 4NS
ENGLAND

1 D. Taylor
Alternative Energy Group
Walton Hall
Open University
Milton Keynes MK7 6AA
ENGLAND

1 P. W. Bach
Netherlands Energy Research Foundation,
ECN
P.O. Box 1
NL-1755 ZG Petten
THE NETHERLANDS

1 J. Beurskens
Programme Manager for Renewable Energies
Netherlands Energy Research Foundation
ECN
Westerduinweg 3
P.O. Box 1
1755 ZG Petten (NH)
THE NETHERLANDS

1 O. de Vries
National Aerospace Laboratory
Anthony Fokkerweg 2
Amsterdam 1017
THE NETHERLANDS

1 J. B. Dragt
Institute for Wind Energy
Faculty of Civil Engineering
Delft University of Technology
Stevinweg 1
2628 CN Delft
THE NETHERLANDS

1 R. A. Galbraith
Dept. of Aerospace Engineering
James Watt Building
University of Glasgow
Glasgow G12 8QG
SCOTLAND

1 M. G. Real, President
Alpha Real Ag
Feldeggstrasse 89
CH 8008 Zurich
SWITZERLAND

1	MS	0167	C. Miller, 12621
1	MS	0443	H. S. Morgan, 9117/9118
50	MS	0708	H. M. Dodd, 6214
1	MS	0708	T. D. Ashwill, 6214
1	MS	0708	D. E. Berg, 6214
1	MS	0708	M. A. Rumsey, 6214
1	MS	0708	H. J. Sutherland, 6214
1	MS	0708	P. S. Veers, 6214
1		0833	J. H. Biffle, 9103 Route to: 9111, 9115
1		0836	C. W. Peterson, 9116 Route to: 9112, 9113, 9114
1	MS	0836	J. H. Strickland, 9116
5		0836	W. P. Wolfe, 9116
1		0841	P. J. Hommert, 9100
1		9018	Central Files, 8940-2
5		0899	Technical Lebrary, 4916
2		0619	Review & Approval Desk, 12690 For DOE/OSTI